More is not always better: finding the right trade-off between affinity and selectivity of a G4 ligand

Michela Zuffo[1], Aurore Guédin[2], Emma-Dune Leriche[2], Filippo Doria[1], Valentina Pirota[1], Valérie Gabelica[2], Jean-Louis Mergny[2,3,*] and Mauro Freccero[1,*]

[1] Dipartimento di Chimica, Università di Pavia, Pavia, 27100, Italy
[2] ARNA Laboratory, Université de Bordeaux, Inserm U1212, CNRS UMR5320, Institut Européen de Chimie Biologie (IECB), Pessac, 33607, France
[3] Institute of Biophysics, AS CR, Brno, 61265, Czech Republic

* To whom correspondence should be addressed. Tel: +390382987668; Fax: +390382987323; Email: mauro.freccero@unipv.it
Correspondence may also be addressed to Tel: +33540003022; Fax: +33540003004; Email: jean-louis.mergny@inserm.fr

Present Address: Michela Zuffo, Institut Curie, CNRS UMR9187, INSERM U1196, PSL Research University, Orsay, 91400, France

Contents

Table S1 Nucleic acid sequences used in the present study p. S2
Table S2 Labelled nucleic acid sequences used for FRET melting assays p. S2
Table S3 Competitor nucleic acid sequences used for FRET melting assays p. S2
Fig. S1 Aggregation experiments in methanol p. S3
Fig. S2 Aggregation experiments in DMSO p. S3
Fig. S3 Aggregation constants calculation p. S4
Fig. S4 Experiments at variable solvent composition p. S5
Fig. S5 Absorption spectra in SDS p. S5
Fig. S6 Ionic strength-dependent experiments for c_{ex}-NDI **1** p. S6
Fig. S7 Spectrophotometric pH-dependent titration for c_{ex}-NDI **1** p. S6
Fig. S8 Temperature-dependent experiments for c_{ex}-NDI **1** p. S7
Fig. S9 Ionic strength-dependent experiments for c_{ex}-NDI **2** p. S7
Fig. S10 Temperature-dependent experiments for c_{ex}-NDI **2** p. S8
Fig. S11 pH-dependent experiments for c_{ex}-NDI **2** p. S8
Fig. S12 FRET experiments with various NA competitors p. S9
Fig. S13 FID assay on Pu24 with c_{ex}-NDI **2** p. S9
Fig. S14 FID assay monitored by native MS p. S10
Fig. S15 Fluorescence titrations on c_{ex}-NDI **2** with parallel G4s p. S11
Tab. S4 Statistical analysis of fluorescence light-up factors p. S11
Fig. S16 Fitting of fluorescence titrations data p. S12
Fig. S17 LOD calculation p. S12
Fig. S18 CD titrations of selected NAs with c_{ex}-NDI **1** and **2** p. S13
Fig. S19 Native gels staining with SYBR Gold p. S13
Fig. S20 Fluorescence titrations of 26TTA and Pu24 with c_{ex}-NDI **1** and **2** p. S14
Fig. S21 CD titrations of 26TTA and Pu24 with c_{ex}-NDI **1** and **2** p. S14
Fig. S22 MS experiments on 26TTA and Pu24 mixtures with c_{ex}-NDI **1** p. S15
HPLC purity data p. S16-18
NMR spectra p. S19-24

Table S1. Nucleic acid sequences used in the present studies. a) auto-complementary duplex. DNA and RNA sequences start with 5'-d and 5'-r, respectively.

Nucleic acid	Sequence	Length	Topology
25Ceb	5'-d(AGGGTGGGTGTAAGTGTGGGTGGGT)-3'	25	Parallel (1)
c-myc	5'-d(TGAGGGTGGGTAGGGTGGGTAA)-3'	22	Parallel (2)
32KRAS	5'-d(AGGGCGGTGTGGGAAGAGGGAAGAGGGGGAGG)-3'	32	Parallel (2)
22AG	5'-d(AGGGTTAGGGTTAGGGTTAGGG)-3'	22	Hybrid (2)
21CTA	5'-d(GGGCTAGGGCTAGGGCTAGGG)-3'	21	Anti-parallel (3)
Bom17	5'-d(GGTTAGGTTAGGTTAGG)-3'	17	Anti-parallel (4)
TBA 15	5'-d(GGTTGGTGTGGTTGG)-3'	15	Anti-parallel (5)
ds26	5'-d(CAATCGGATCGAATTCGATCCGATTG)-3'	26	Duplex DNA (2)[a]
Pu24	5'-d(TGAGGGTGGGGAGGGTGGGGAAGG)-3'	24	Parallel (6)
hRAS1	5'-d(TCGGGTTGCGGGCGCAGGGCACGGGCG)-3'	27	Anti-paralleL (7)
ss SCR	5'-d(GGATGTGAGTGTGAGTGTGAGG)-3'	22	Single strand (2)
VAV1	5'-d(GGGCAGGGAGGGAACTGGG)-3'	19	Parallel (7)
VEGF	5'-d(GGGAGGGTTGGGGTGGG)-3'	17	Parallel (5)
c-kit2	5'-d(CCCGGGCGGGCGCGAGGGAGGGGAGG)-3'	26	Parallel (2)
c-kit1	5'-d(AGGGAGGGCGCTGGGAGGAGGG)-3'	22	Parallel (2)
Bcl2	5'-d(GGGCGGGCGCGGGAGGAAGGGGGCGGG)-3'	27	Parallel (5)
TERRA	5'-r(AGGGUUAGGGUUAGGGUUAGGG)-3'	22	Parallel (3)
NRAS	5'-r(UGUGGGAGGGGCGGGUCUGGG)-3'	21	Parallel (8)
ss37	5'-d(GTTTAGTTTAGTTTAGTTTAGTTTAGTTTAGTTTAGT)-3'	37	Single strand
mir122	5'-r(UGGAGUGUGACAUGGUGUUUG)-3'	21	Single strand
SL2	5'-r(UCACGGCUAGCUGUGAAAGGUCCGGUGA)-3'	28	Hairpin
26TTA	5'-d(TTAGGGTTAGGGTTAGGGTTAGGGTT)-3'	26	Hybrid (9)

Table S2. Labelled DNA sequences used in the present study. All sequences are provided in the 5' => 3' direction, F = FAM, T = TAMRA.

Labelled DNA	Sequence	Topology (4)
F25CebT	F-AGGGTGGGTGTAAGTGTGGGTGGG-T	Parallel
FmycT	FAM-TTGAGGGTGGGTAGGGTGGGTAA-T	Parallel
F32KRAST	F- AGGGCGGTGTGGGAAGAGGGAAGAGGGGGAGG-T	Parallel
FBom17T	F-GGTTAGGTTAGGTTGG-T	Anti-parallel
F21CTAT	F-GGGCTAGGGCTAGGGCTAGGG-T	Anti-parallel
FTBAT	F-GGTTGGTGTGGTTGG-T	Anti-parallel
F21T	F-GGGTTAGGGTTAGGGTTAGGG-T	Hybrid
FdxT	F-TATAGCTAT-hexaethyleneglycol-ATAGCTATA-T	Hairpin duplex

Table S3. DNA Competitor sequences used in the present study

Nucleic acid	Sequence	Topology
ds26	5'-d(CAATCGGATCGAATTCGATCCGATTG)-3'	Auto-complementary duplex
dx	5'-d(TATAGCTATA-hexaethyleneglycol-TATAGCTATA)-3'	Hairpin duplex
dx12 a dx12 b	5'-d(GCGTGAGTTCGG)-3' 5'-d(CCGAACTCACGC)-3'	Duplex
Bom37mut	5'-d(GTTTAGTTTAGTTTAGTTTAGTTTAGTTTAGT)-3'	Single strand

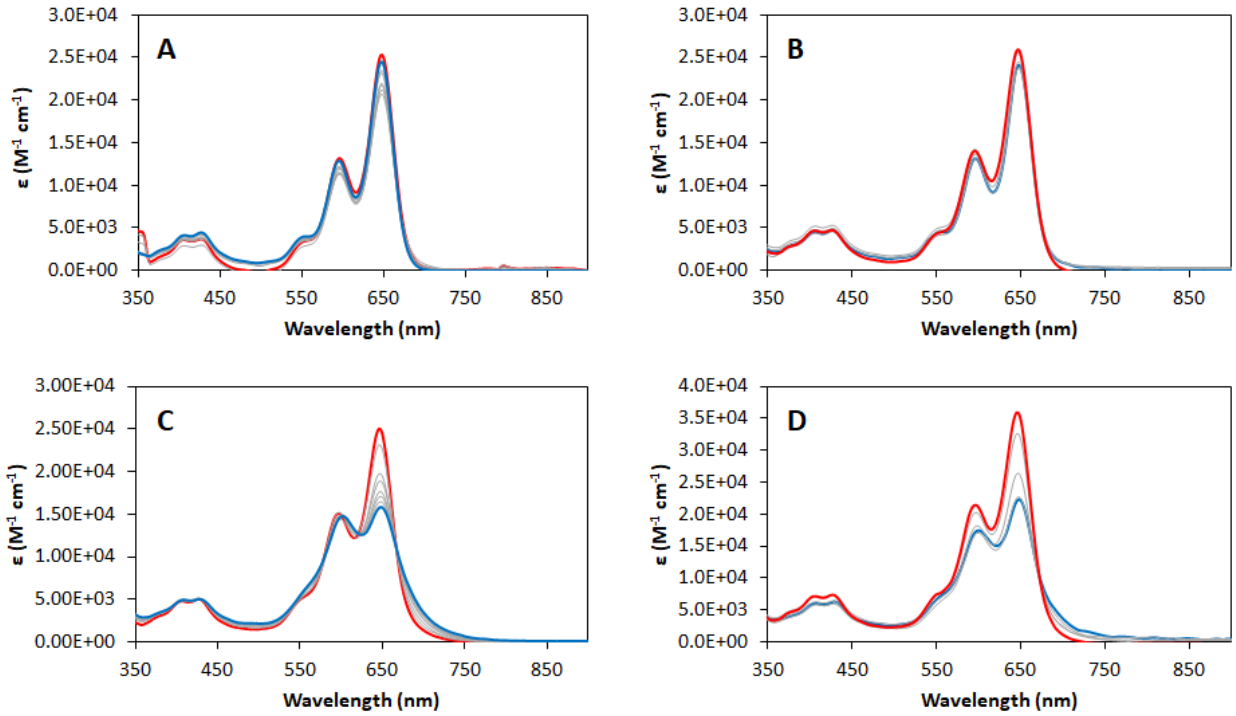

Figure S1. Concentration and temperature dependent experiments conducted in methanol. A) Absorption spectra recorded on a solution of c_{ex}-NDI **1** varying its concentration between $5x10^{-6}$ and $7x10^{-5}$ M; B) absorption spectra recorded on a $1x10^{-5}$ M solution of $_{ex}$-NDI **1** varying the temperature between 5 and 60°C; C) the same as A, using c_{ex}-NDI **2**; D) the same as B, using c_{ex}-NDI **2**. In all graphs the blue curve represents the initial spectrum (low concentration or temperature) and the red curve represents the final one (high concentration or temperature).

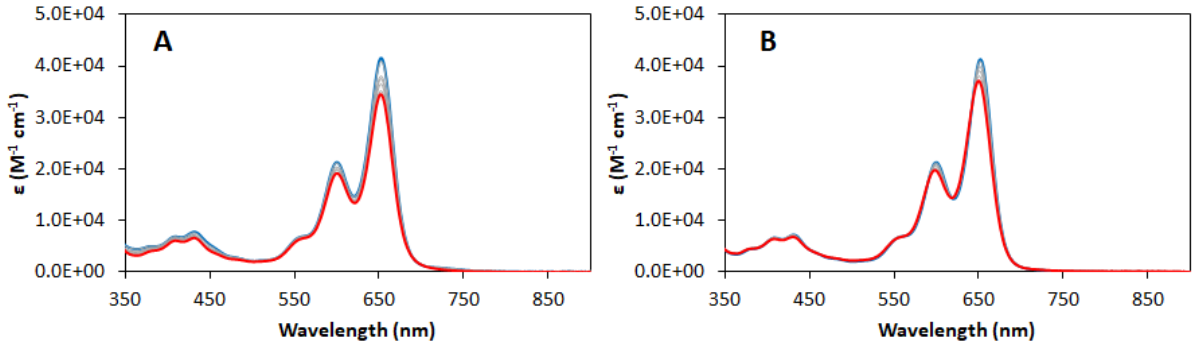

Figure S2. Concentration and temperature dependent experiments conducted in DMSO on c_{ex}-NDI **2**. A) Absorption spectra recorded varying c_{ex}-NDI **2** concentration between $5x10^{-6}$ and $6x10^{-5}$ M; B) absorption spectra recorded on a $1x10^{-5}$ M solution of $_{ex}$-NDI **2** varying the temperature between 20 and 70°C. In both graphs the blue curve represents the initial spectrum (low concentration or temperature) and the red curve represents the final one (high concentration or temperature).

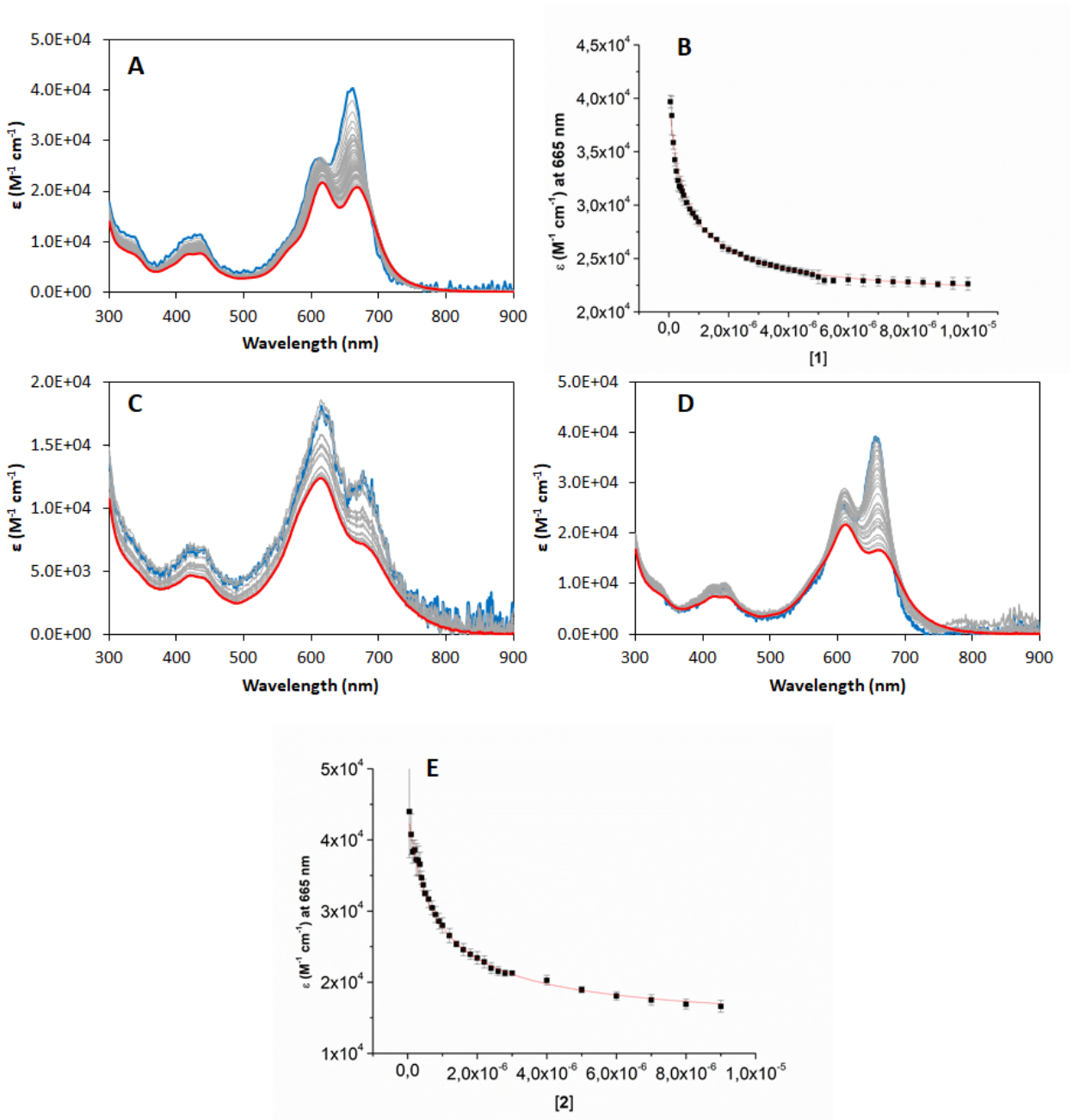

Figure S3. Aggregation constants calculation. A) Absorption spectra of a solution of c_{ex}-NDI **1** in water ($1x10^{-2}$ M TRIS-HCl buffer, pH 7.2), recorded while varying its concentration between $5x10^{-8}$ and $1x10^{-5}$ M; B) isodesmic fitting of the molar absorptivity coefficient data at 665 nm obtained from A; C) the same as A, with c_{ex}-NDI **2**; D) absorption spectra of a solution of c_{ex}-NDI **1** in water and methanol (1:1 mixture, $1x10^{-2}$ M TRIS-HCl buffer, pH 7.2), recorded while varying its concentration between $5x10^{-8}$ and $9x10^{-6}$ M; E) isodesmic fitting of the molar absorptivity coefficient data at 665 nm obtained from D.

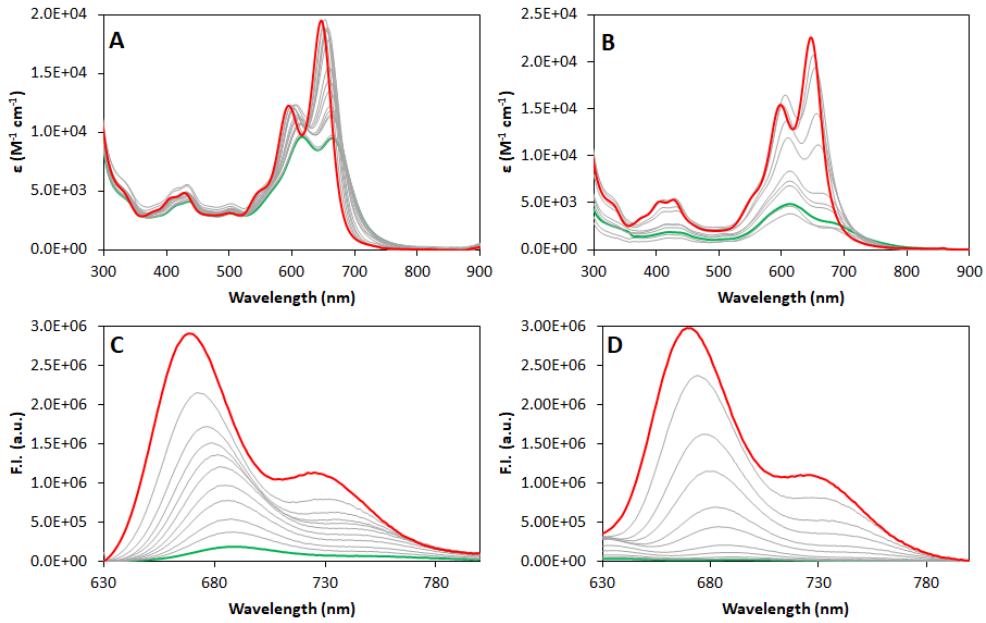

Figure S4. A) Absorption spectra of $2x10^{-5}$ M solutions of c_{ex}-NDI **1** in MeOH-water mixtures at varying compositions (0-100%); B) the same as A, with c_{ex}-NDI **2**; C) Emission spectra of $5x10^{-6}$ of c_{ex}-NDI **1** in MeOH-water mixtures at varying compositions (0-100%) (λ_{exc} = 620 nm); D) the same as C, with c_{ex}-NDI **2**. Green: pure water, Red: pure methanol. pH was fixed in water at 7.2 with $1x10^{-2}$ M lithium cacodylate buffer.

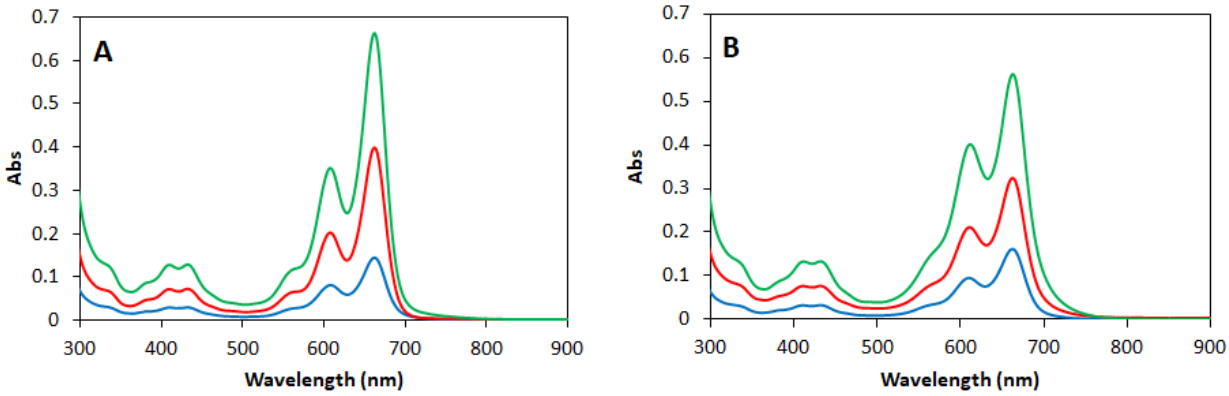

Figure S5. Absorption spectra of $2X10^{-2}$ M SDS water solutions of A) c_{ex}-NDI **1** B) c_{ex}-NDI **2**. pH was fixed at 7.2 with $1x10^{-2}$ M lithium cacodylate buffer. Compounds concentration: blue = $5x10^{-6}$ M, red = $1x10^{-5}$ M, blue = $2x10^{-5}$ M.

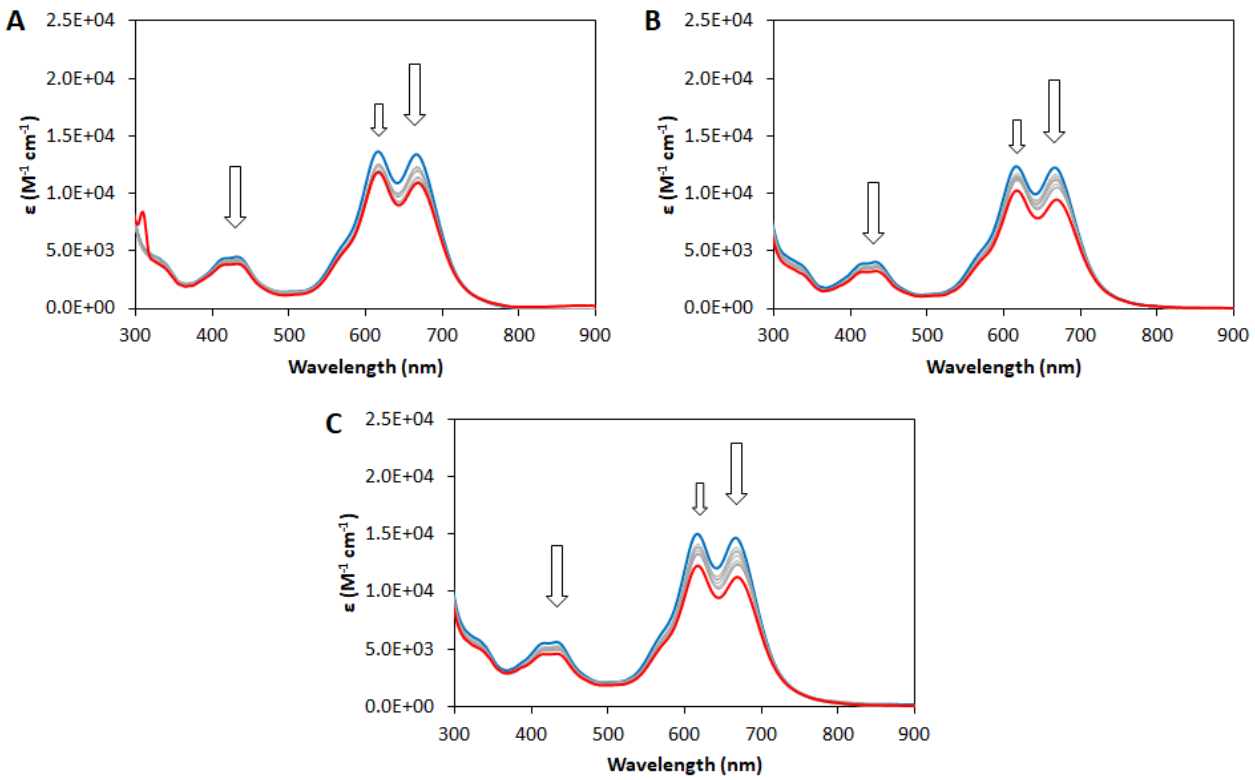

Figure S6. Absorption spectra of 1x10^{-5} M solutions of c_{ex}-NDI **1** in water (pH 7.2, 1x10^{-2} M TRIS-HCl buffer) with 0-2x10^{-1} M A) KCl, B) NaCl, C) LiCl. Blue: no salt; Red 2x10^{-1} M salt.

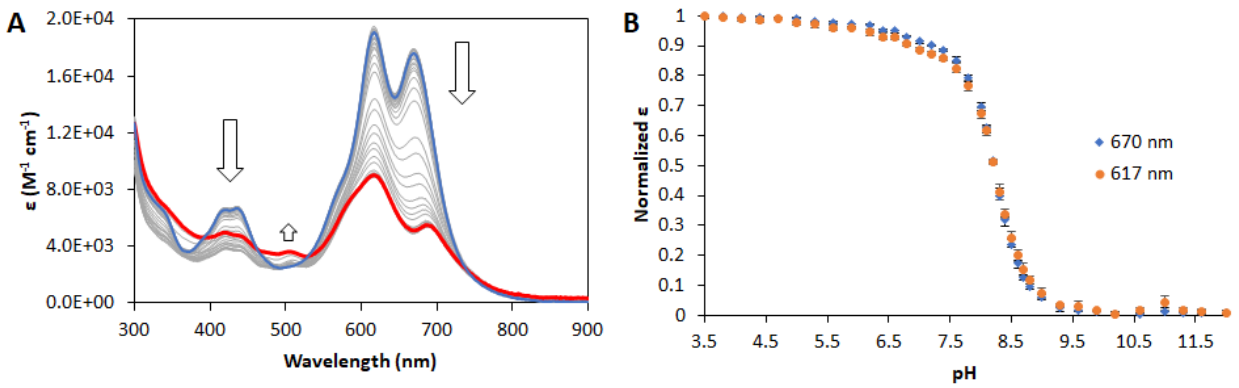

Figure S7. A) Absorption spectra of a 1x10^{-5} M solution of c_{ex}-NDI **1** in water recorded while gradually varying the pH from 3.5 to 12 with the addition of NaOH; B) normalized molar absorptivity coefficient data in the two maxima (617 and 670 nm), plotted as a function of pH.

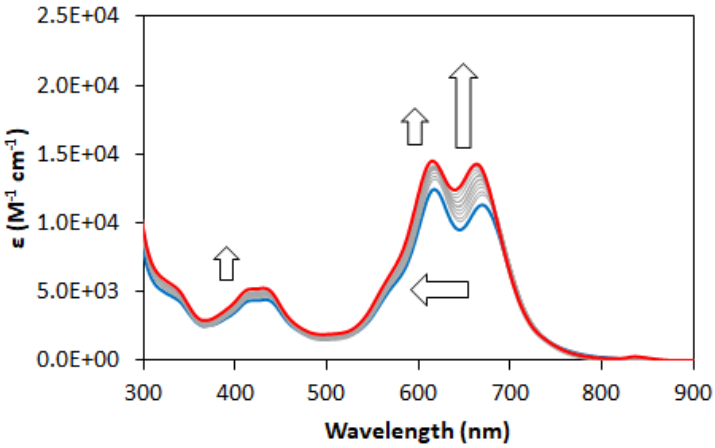

Figure S8. Absorption spectra of a $2x10^{-5}$ M solution of compound **1** in water (pH 7.2, $1x10^{-2}$ M lithium cacodylate buffer, $1x10^{-1}$ M KCl) at increasing temperature (25-95°C). Blue = 25°C, Red = 95°C.

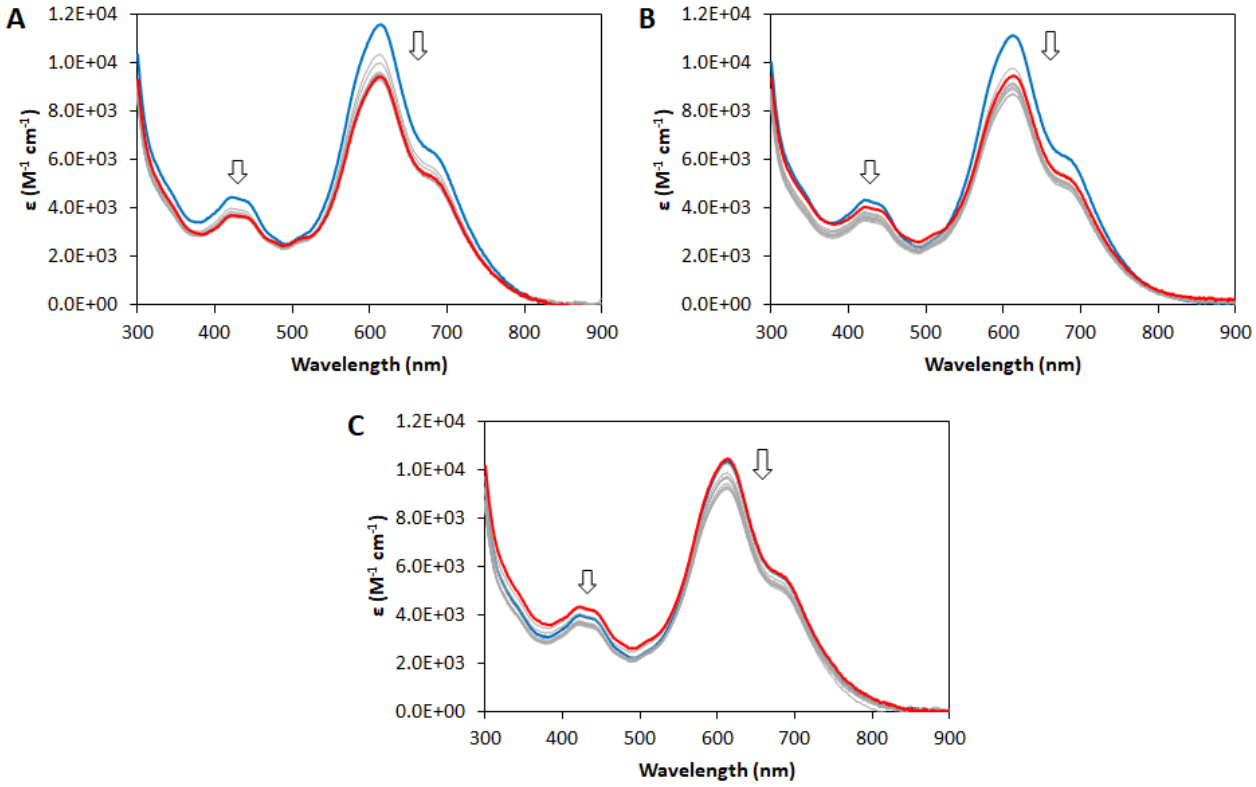

Figure S9. Absorption spectra of $1x10^{-5}$ M solutions of c_{ex}-NDI **2** in water (pH 7.2, $1x10^{-2}$ M TRIS-HCl buffer) with 0-$2x10^{-1}$ M A) KCl, B) NaCl, C) LiCl. Blue: no salt; Red: $2x10^{-1}$ M salt.

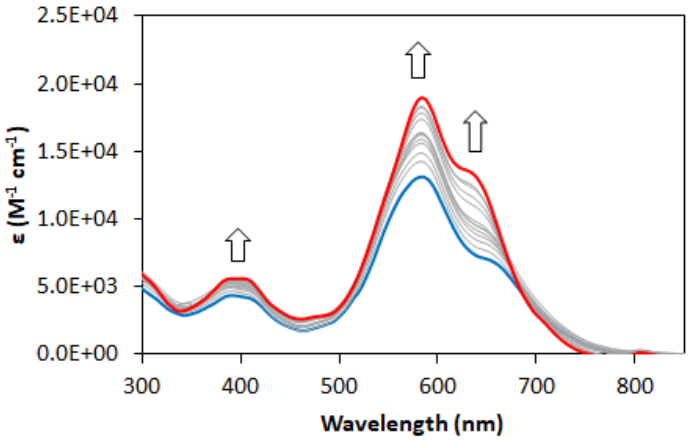

Figure S10. Absorption spectra of a $2x10^{-5}$ M solution of compound **2** in water (pH 7.2, $1x10^{-2}$ M lithium cacodylate buffer, $1x10^{-1}$ M KCl) at increasing temperature (25-95°C). Blue = 25°C, Red = 95°C.

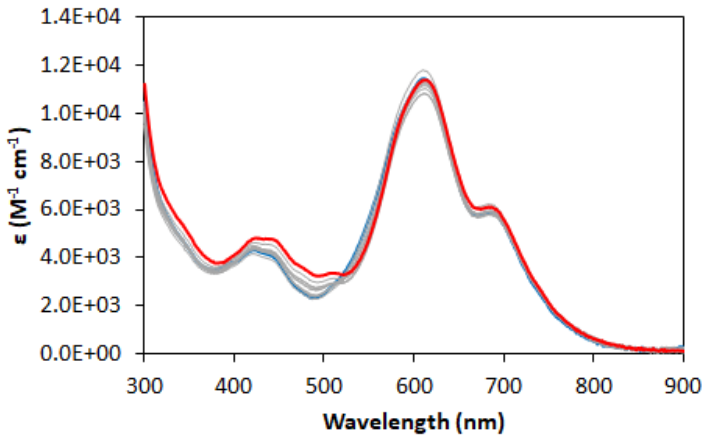

Figure S11. Absorption spectra of $1x10^{-5}$ M solutions of c_{ex}-NDI **2** in water ($1x10^{-2}$ M buffer, either phosphoric acid-sodium dihydrogenphosphate, or sodium dihydrogenphosphate-sodium monohydrogenphosphate, or sodium monohydrogenphosphate-sodium phosphate) at increasing pH (from 2 to 12). Blue = pH 2; Red = pH 12.

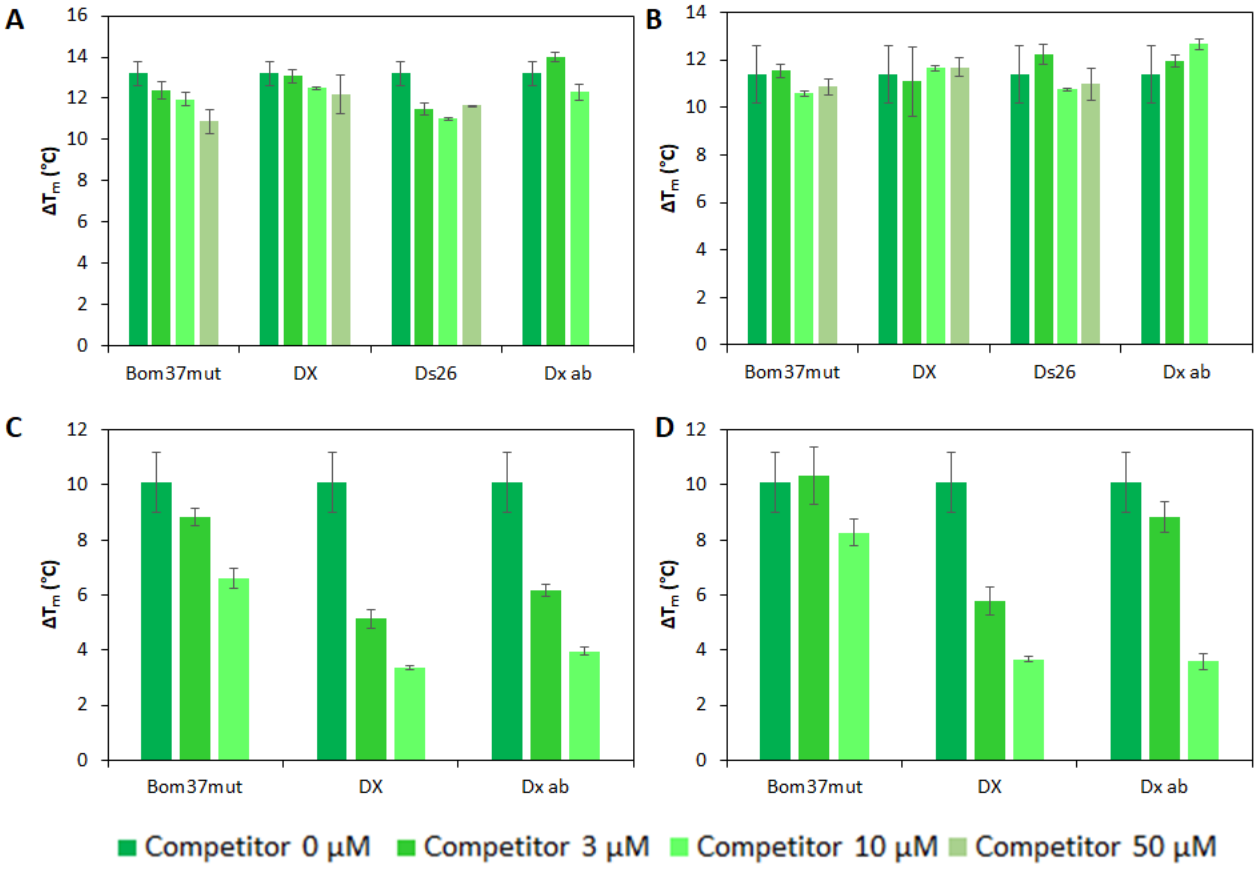

Figure S12. Results of FRET melting assays carried out in lithium cacodylate buffer $1x10^{-2}$ M, pH 7.2, KCl $1x10^{-3}$ M and LiCl $9.9x10^{-2}$ M on $2x10^{-6}$ M nucleic acid with increasing amounts of competitors ($0-5x10^{-5}$ M). A) 25Ceb with ligand **2** ($5x10^{-6}$ M); B) c-myc with ligand **2** ($5x10^{-6}$ M); C) 25Ceb with ligand **1** ($2.5x10^{-7}$ M); D) c-myc with ligand **1** ($2.5x10^{-7}$ M). Bom37mut = single strand competitor, DX = hairpin duplex, ds26 = auto-complementary duplex, Dx ab = duplex DNA (Tab. S3).

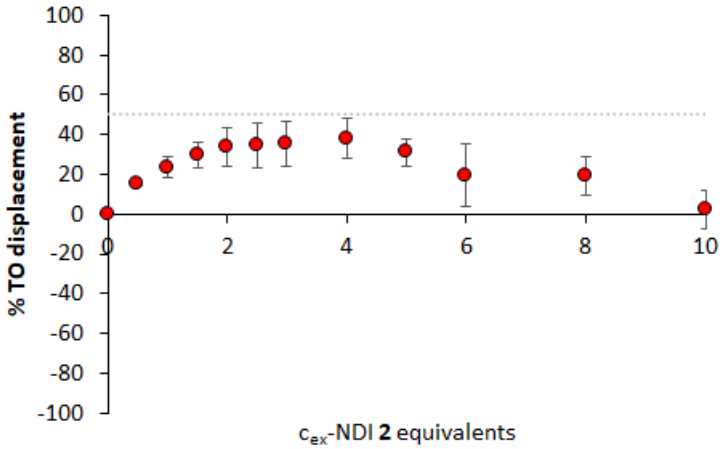

Figure S13. FID assay of c_{ex}-NDI **2** on a Pu24 G4 (pH 7.2, $1x10^{-2}$ M lithium cacodylate buffer, $1x10^{-1}$ M KCl, T = 25°C). Dotted lines indicate 50% displacement.

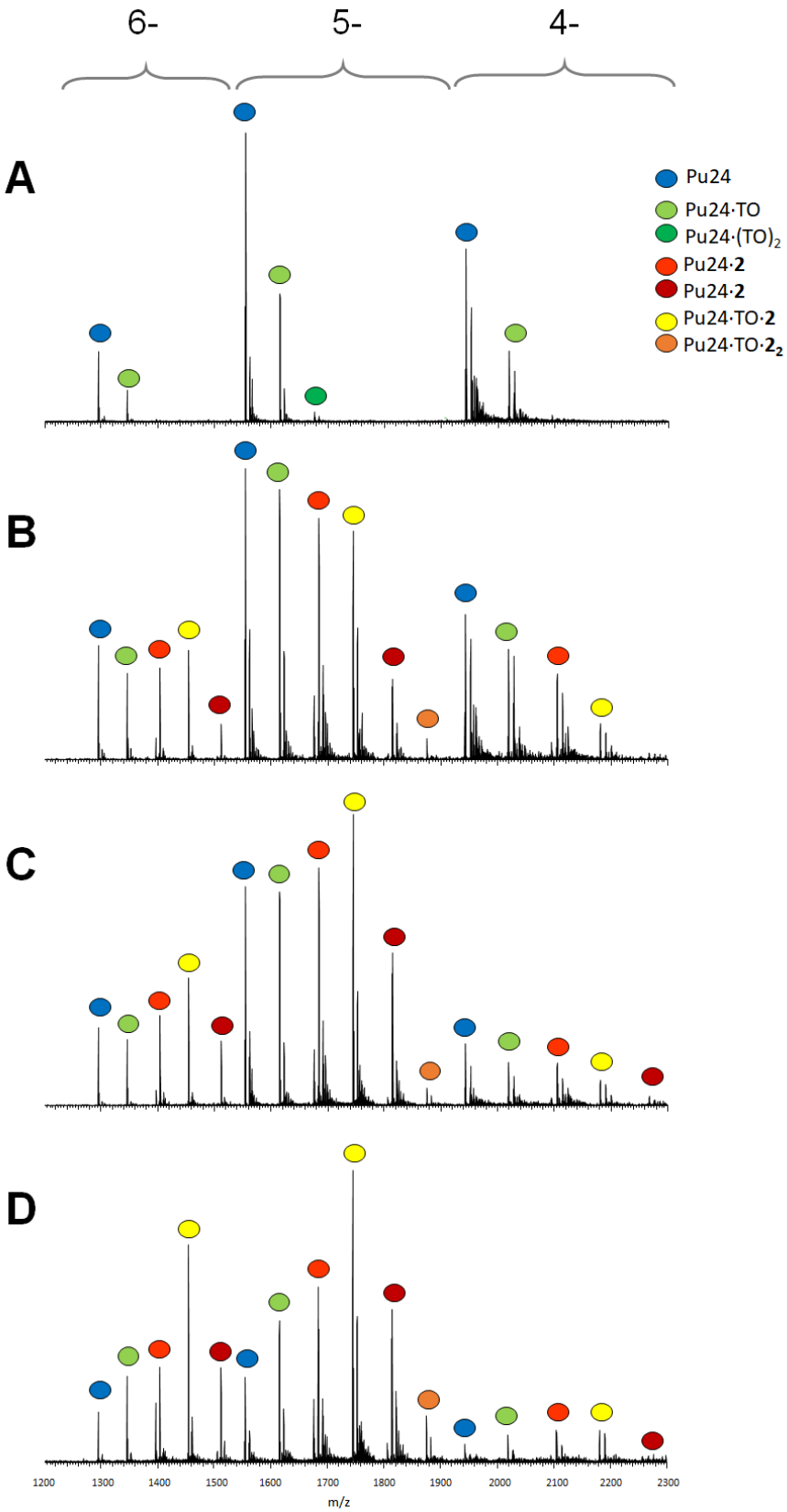

Figure S14. MS analysis of a Pu24 ($5x10^{-6}$ M), TO ($1x10^{-5}$ M), c_{ex}-NDI **2** (0, 10, 25, $50x10^{-6}$ M in A, B, C and D respectively) mixtures (100 mM TMAA, pH 7, 1 mM KCl). All highlighted species contain two K^+ cations in their main peak, in line with the expected 3-quartet G-quadruplex structure.

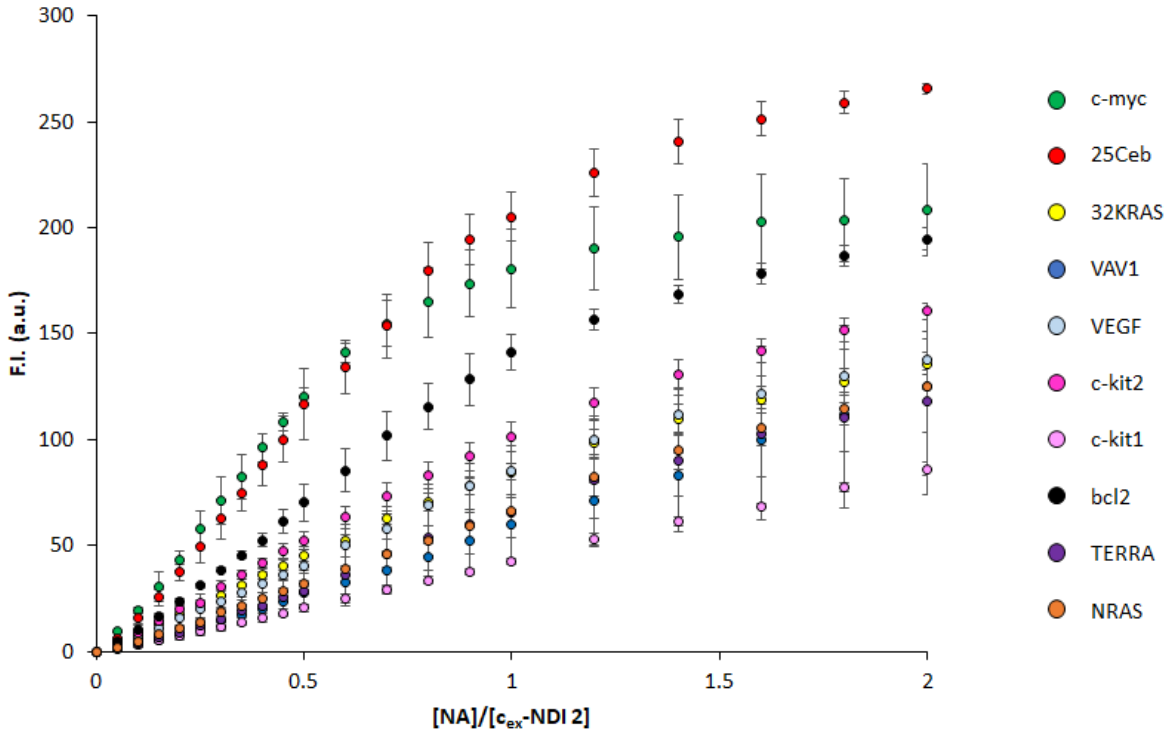

Figure S15. Normalized fluorescence in the maximum (685-695 nm), calculated from fluorescence titrations data of $4x10^{-6}$ M water solutions of c_{ex}-NDI **2** (pH 7.2, $1x10^{-2}$ M TRIS-HCl, $1x10^{-1}$ M KCl, T = 25°C) with an extended panel of parallel G4s, c = 0-$8x10^{-6}$ M.

Table S4. Statistical comparison (T test, equality of variances was verified by F test with $p<0.001$) of fluorescence enhancement factors of c_{ex}-NDIs **1** and **2** in the presence of two equivalents of NA. NAs are grouped and compared as parallel G4s against non-parallel G4s or against non-parallel G4s and controls. a) data correspond to the comparison with the parallel G4s group.

		Parallel G4s	**Non parallel G4s**	**Non-parallel G4s + controls**
c_{ex}-NDI **2**	Average F/F_0-1	155.6	56.9	42.7
	Standard deviation	52.9	30.2	26.1
	Variance	2803.4	683.6	914.9
	T	-	13.4[a]	9.8[a]
	Degrees of freedom	-	12[a]	14[a]
	t critical (p=0.001)	-	4.32[a]	4.14[a]
c_{ex}-NDI **1**	Average F/F_0-1	10.6	10.9	10.9
	Standard deviation	1.4	2.7	2.1
	Variance	2.0	7.4	4.5
	T	-	0.32[a]	0.39[a]
	Degrees of freedom	-	5[a]	7[a]
	t critical (p=0.001)	-	1.476[a]	1.415[a]

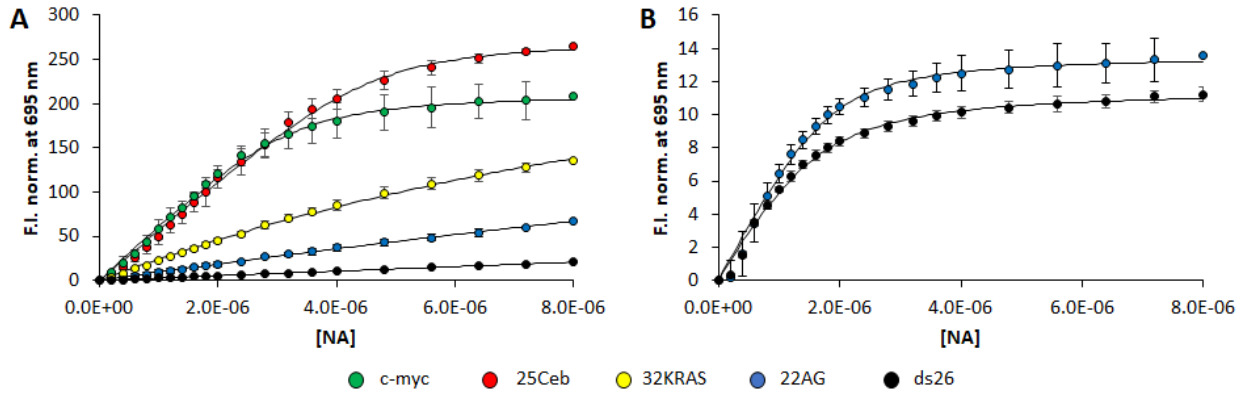

Figure S16. Fitting of titrations of A) c_{ex}-NDI **2** and B) c_{ex}-NDI **1** presented in fig. 5 for selected NAs.

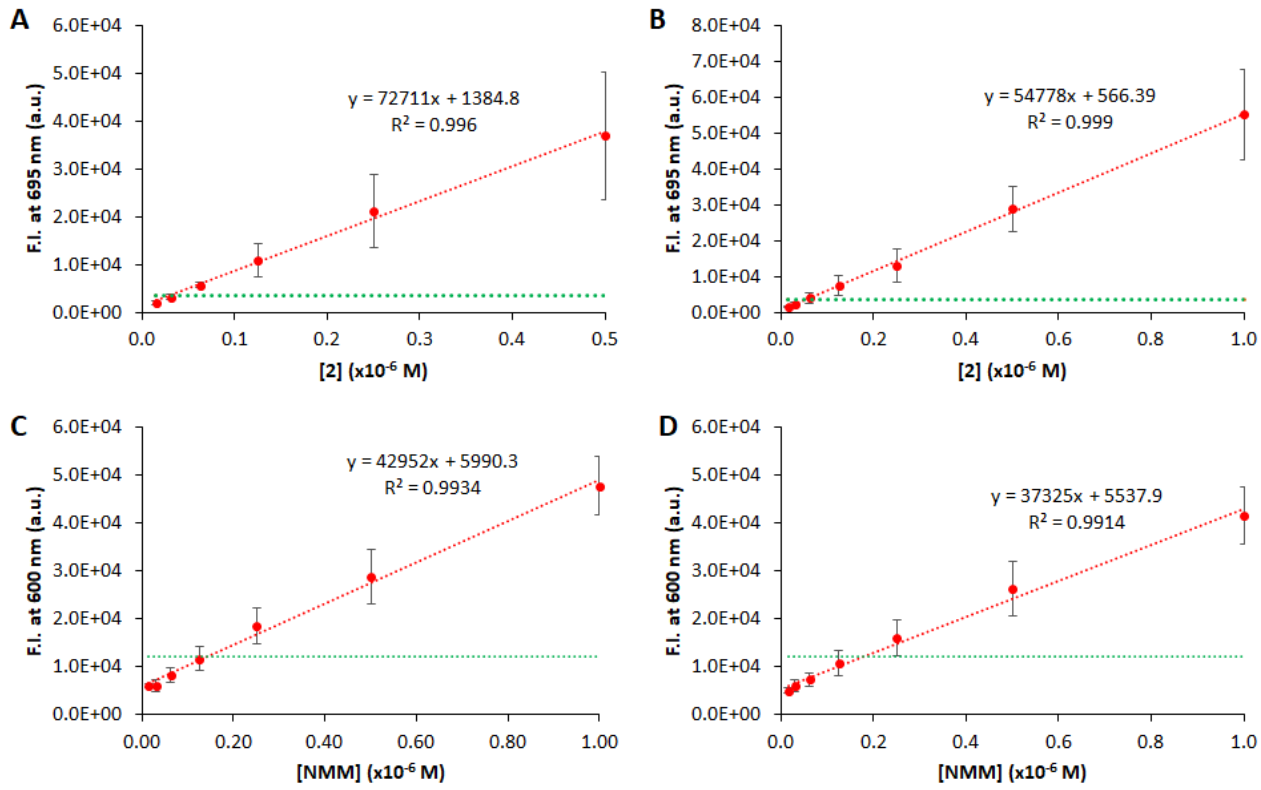

Figure S17. Analysis of the sensitivities of c_{ex}-NDI **2** and NMM in staining the parallel G4s c-myc and 25Ceb. A) sensing of c-myc by **2**; B) sensing of 25Ceb by **2**, C) sensing of c-myc by NMM; D) sensing of 25Ceb by NMM. λ_{exc} (**2**) = 650 nm, λ_{exc} (NMM) = 400 nm, λ_{em} (**2**) = 695 nm, λ_{em} (NMM) = 600 nm. Data are the average of three replicates, each conducted in duplicate conditions. The G4 and compound concentrations varied between 0.1 and $1x10^{-6}$ M. 20 measurements were performed on the compounds alone, in order to obtain a reasonable S_b value to use in the LOD calculation.

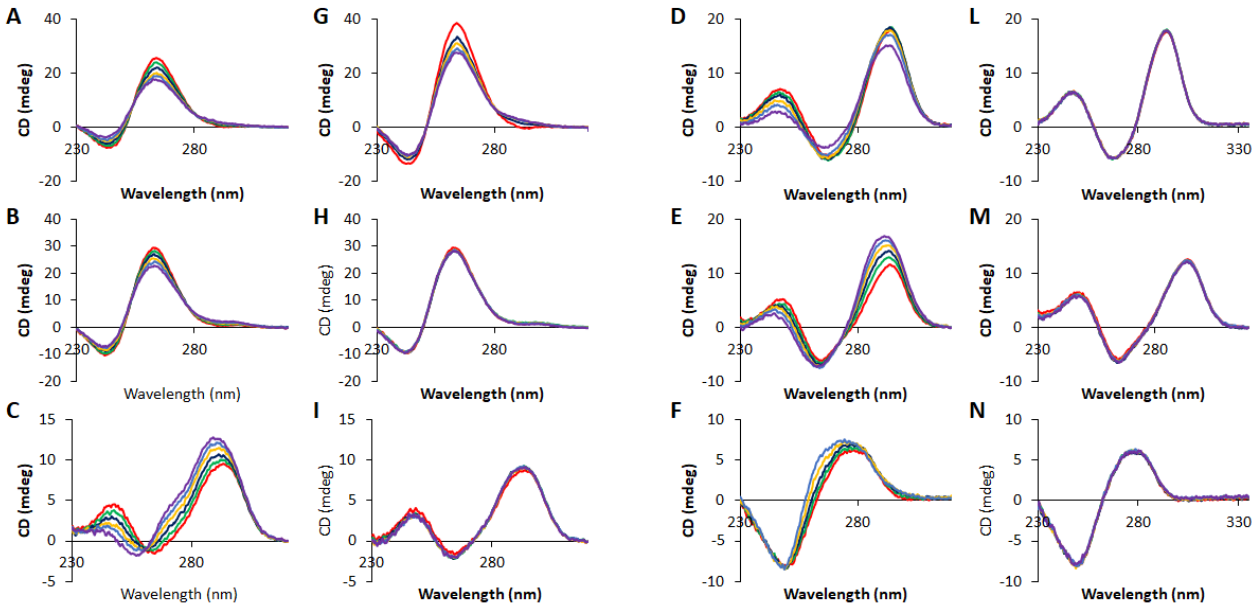

Figure S18. Circular dichroism spectra of $3x10^{-6}$ M solutions (pH 7.2, $1x10^{-2}$ M lithium cacodylate buffer, $1x10^{-1}$ M KCl, T = 25°C) of A,G) 25Ceb; B,H) 32KRAS; C,I) 21CTA; D,L) TBA; E,M) Bom17; F,N) ds26 in the presence of 0-$9x10^{-6}$ M c_{ex}-NDI **1** (A-F) or c_{ex}-NDI **2** (G-N), corresponding to 0-3 molar equivalents. Red: 0 eqv; green: 0.5 eqv; blue: 1 eqv; yellow: 1.5 eqv; light blue: 2 eqv; purple: 3 eqv.

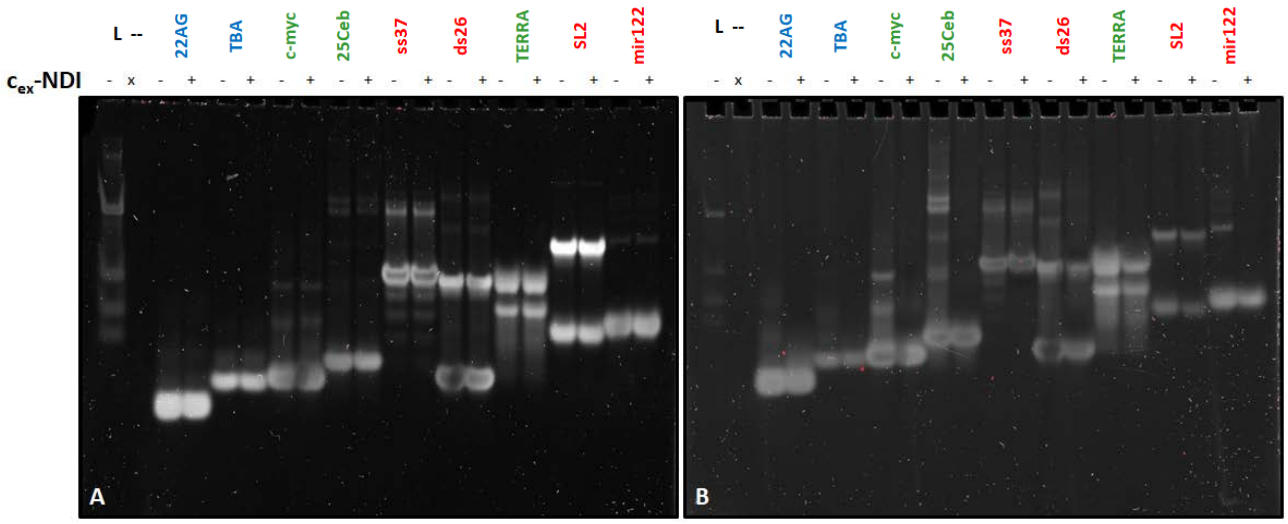

Figure S19. Native gel electrophoretic analysis of solutions containing either the NA alone or the NA with 1 equivalent of c_{ex}-NDI **2** (A) or **1** (B) (NA: 30 pmol, compound: 0-30 pmol, 12% polyacrylamide, 18°C, 2h, 150 V), stained with SYBR Gold. Green: parallel G4s, blue: non-parallel G4s, orange: controls. L = ladder and fluorescent markers.

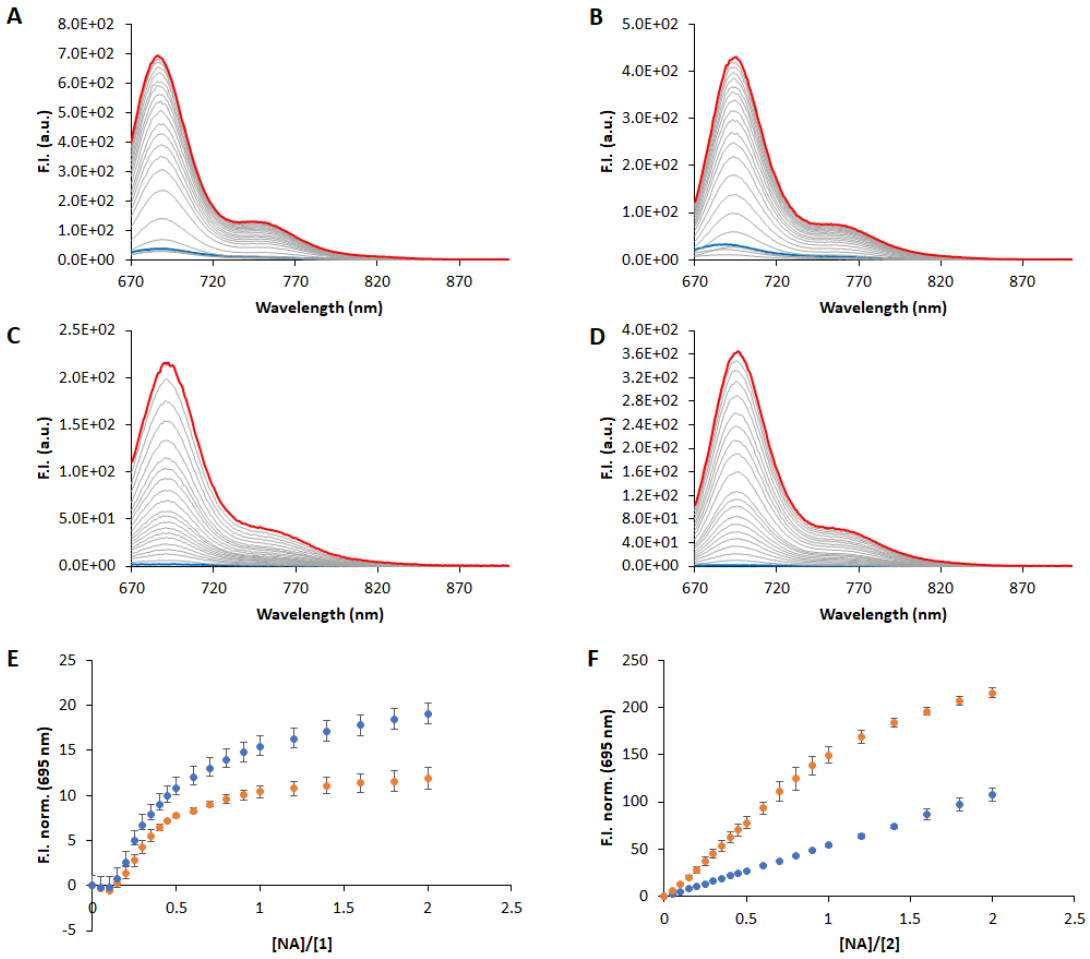

Figure S20. Fluorescence titrations of 26TTA (A and C) and Pu24 (B and D) with **1** (A and B) and **2** (C and D) and associated fluorescence enhancement factors (E: compound **1**, F: compound **2**) ($1x10^{-1}$ M KCl, $1x10^{-2}$ M TRIS-HCl buffer, pH 7.2, $4x10^{-6}$ M c_{ex}-NDI, 0-$8x10^{-6}$ M G4, λ_{exc} = 650 nm).

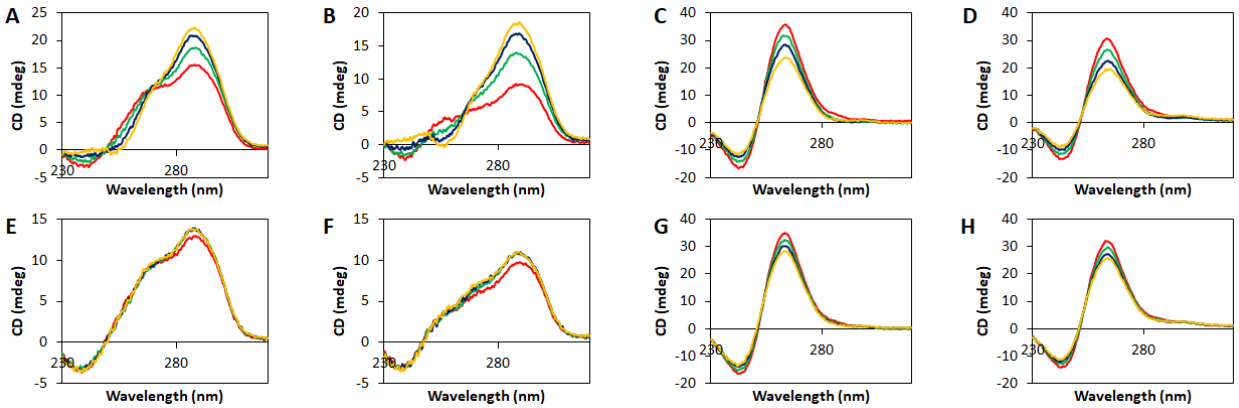

Figure S21. Circular dichroism spectra of $3x10^{-6}$ M solutions (pH 7.2, $1x10^{-2}$ M lithium cacodylate buffer, $1x10^{-1}$ M KCl, T = 25°C) of A,B,E,F) 26TTA; C,D,G,H) Pu24 in the presence of 0-$9x10^{-6}$ M c_{ex}-NDI **1** (A-D) or c_{ex}-NDI **2** (E-H), corresponding to 0-3 molar equivalents. Spectra in graphs A, C, E and G were recorded in $1x10^{-2}$ M lithium cacodylate buffer (pH 7.2) in the presence of $1x10^{-1}$ M KCl, whereas spectra in graphs B, D, F and H were recorded in $1x10^{-1}$ M TMAA buffer (pH 7) in the presence of $1x10^{-3}$ M KCl. Red: 0 eqv; green: 1 eqv; blue: 2 eqv; yellow: 3 eqv.

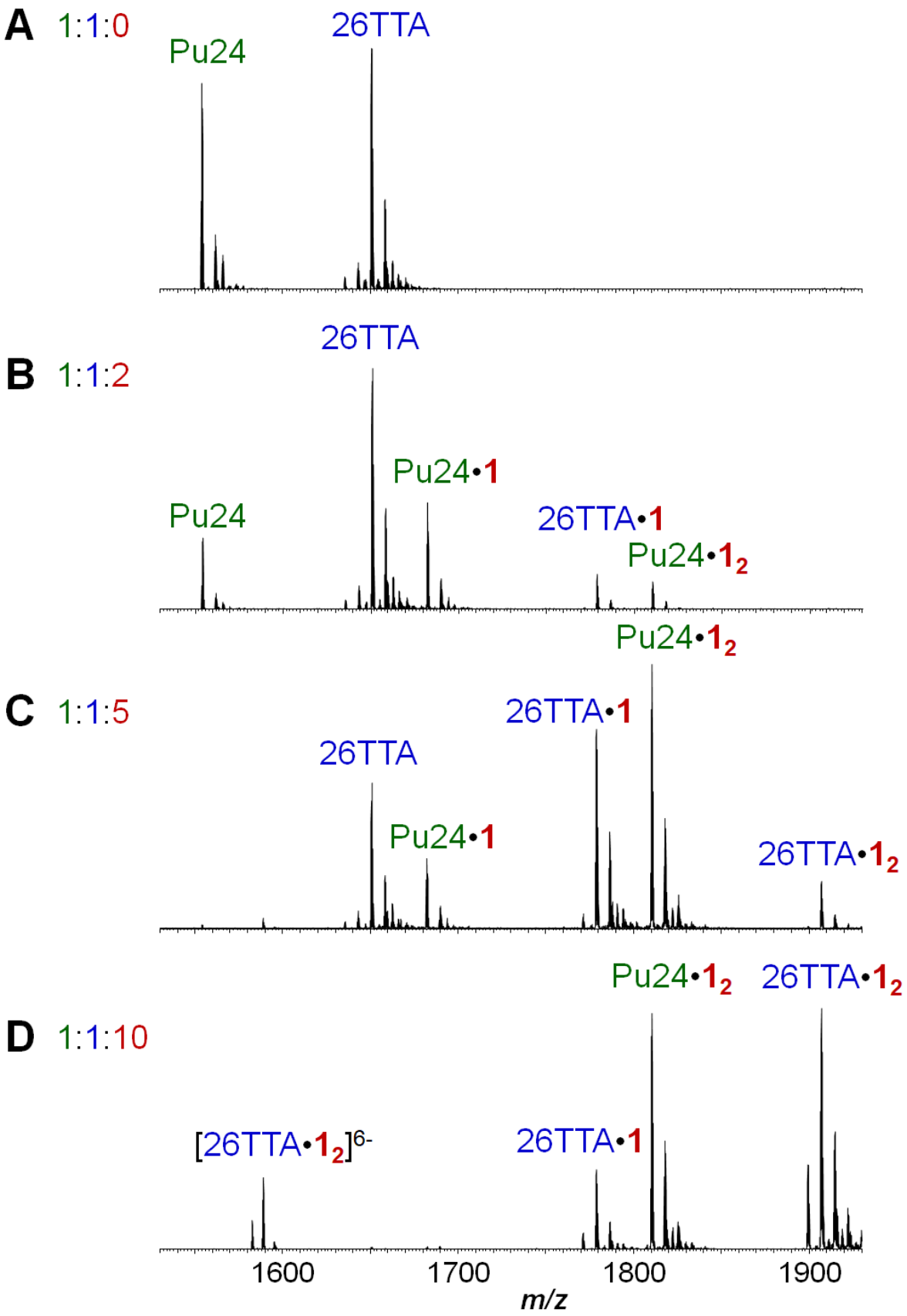

Figure S22. Mass spectra of a 1:1 mixture of Pu24 and 26TTA G4s (5 µM each, 0.1 M TMAA, pH 7, 1 mM KCl) in the presence of increasing amounts of c_{ex}-NDI **1** (0, 2, 5 and 10 molar equivalents).

HPLC purity data

Compound 1

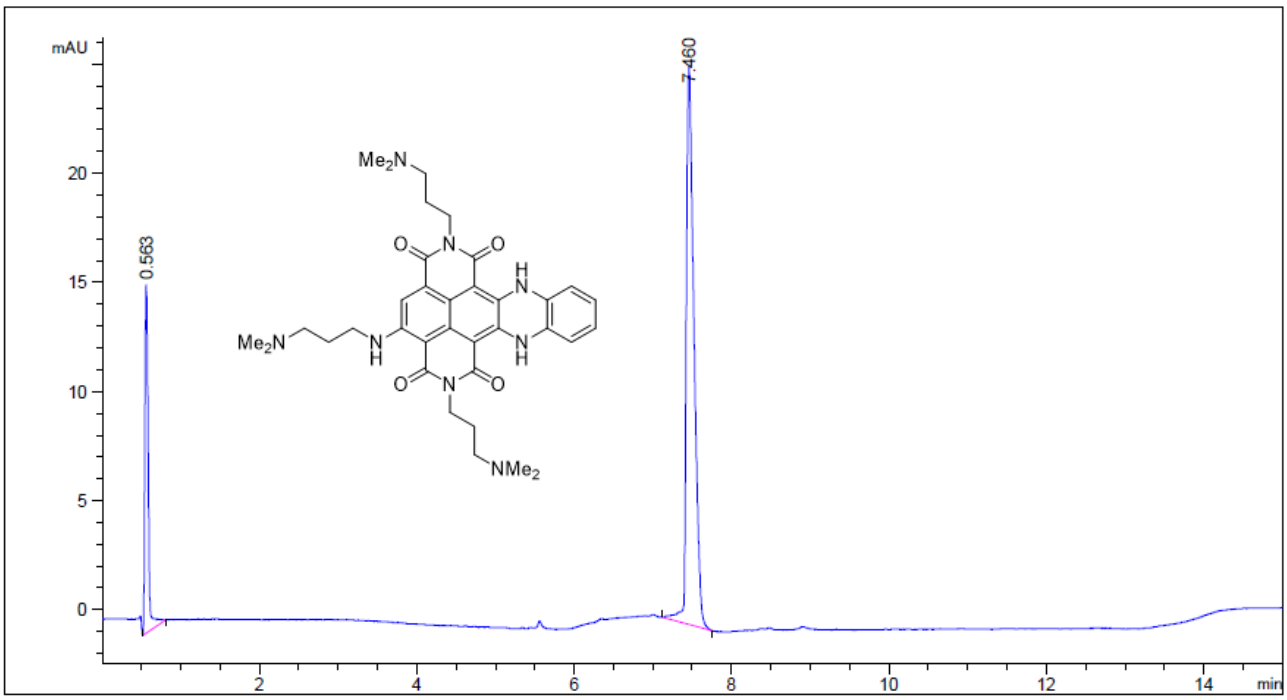

Compound 2

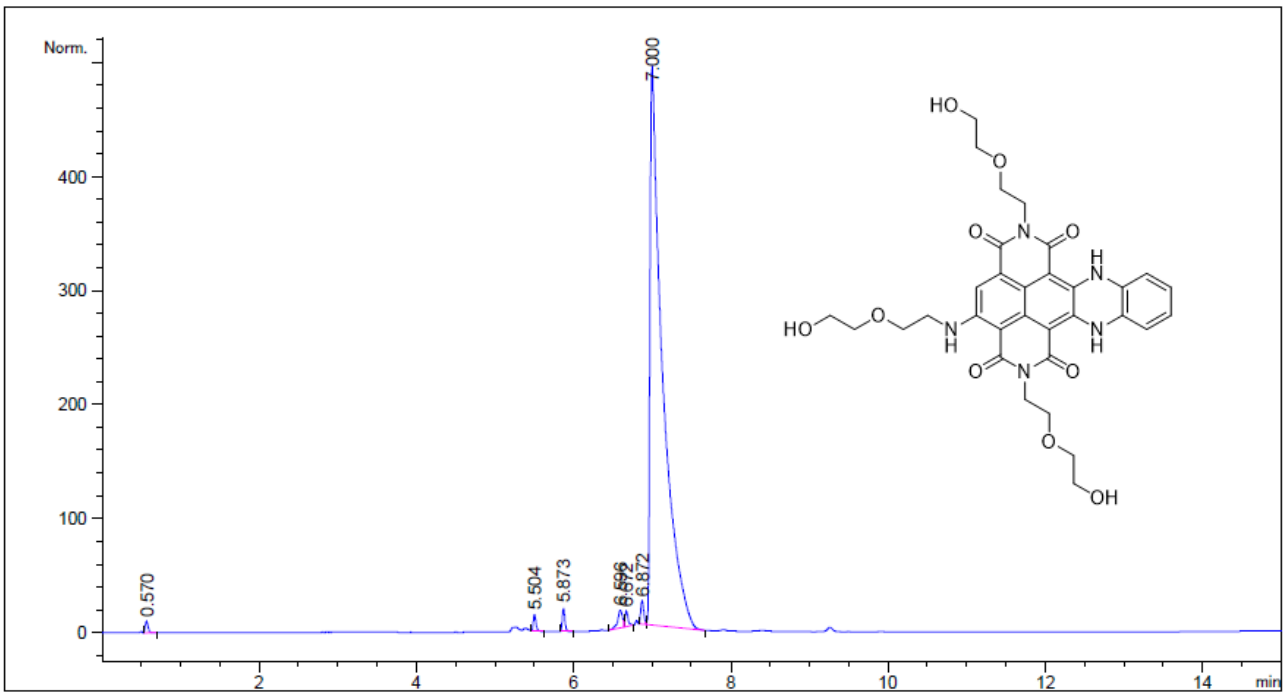

Compound 8

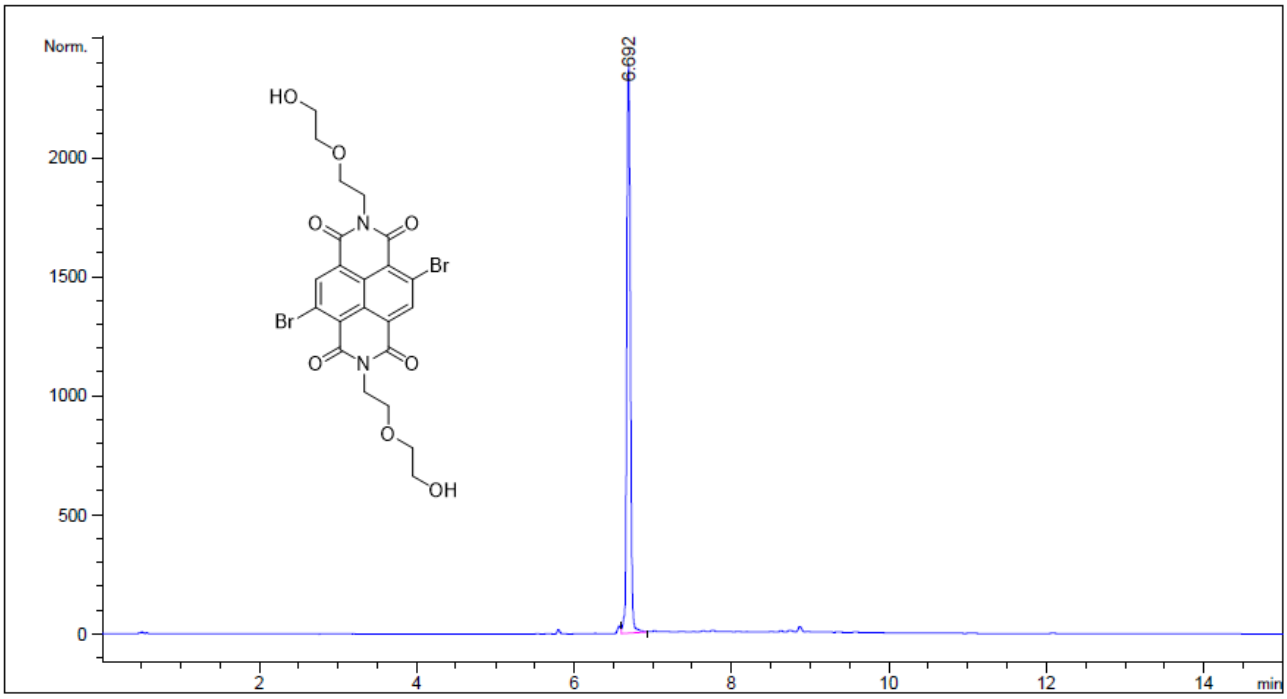

Compound 9

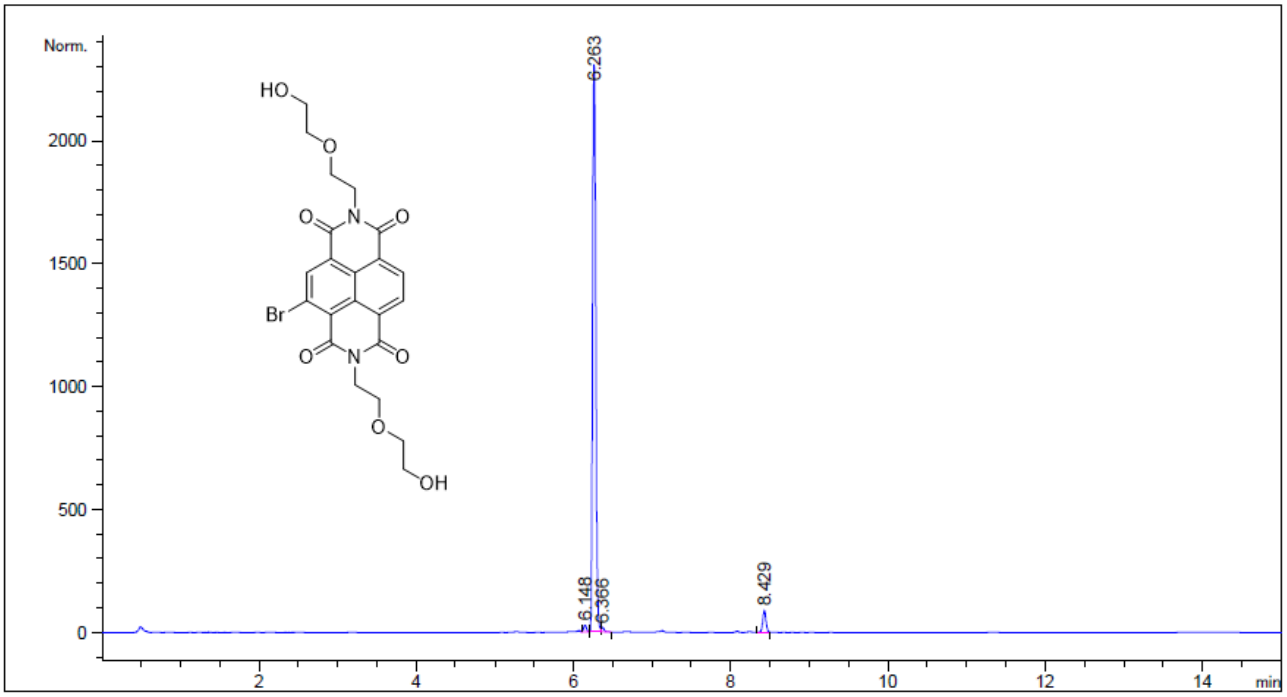

Compound 12

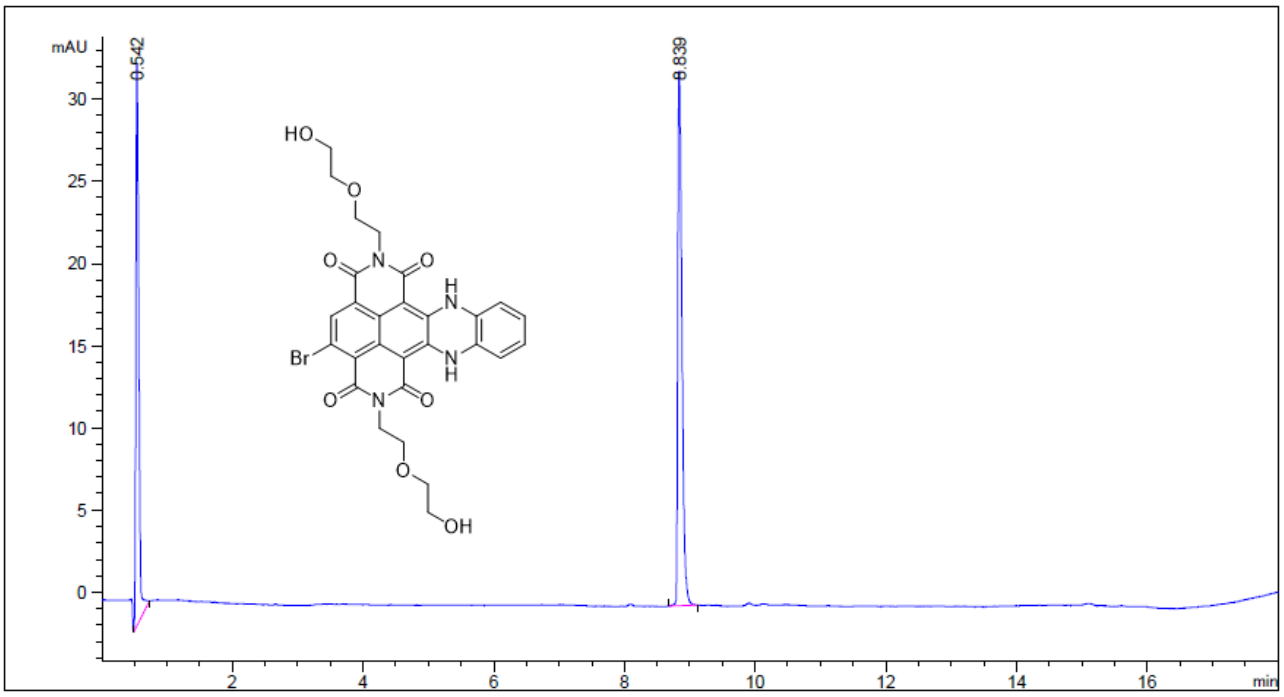

Compound 13

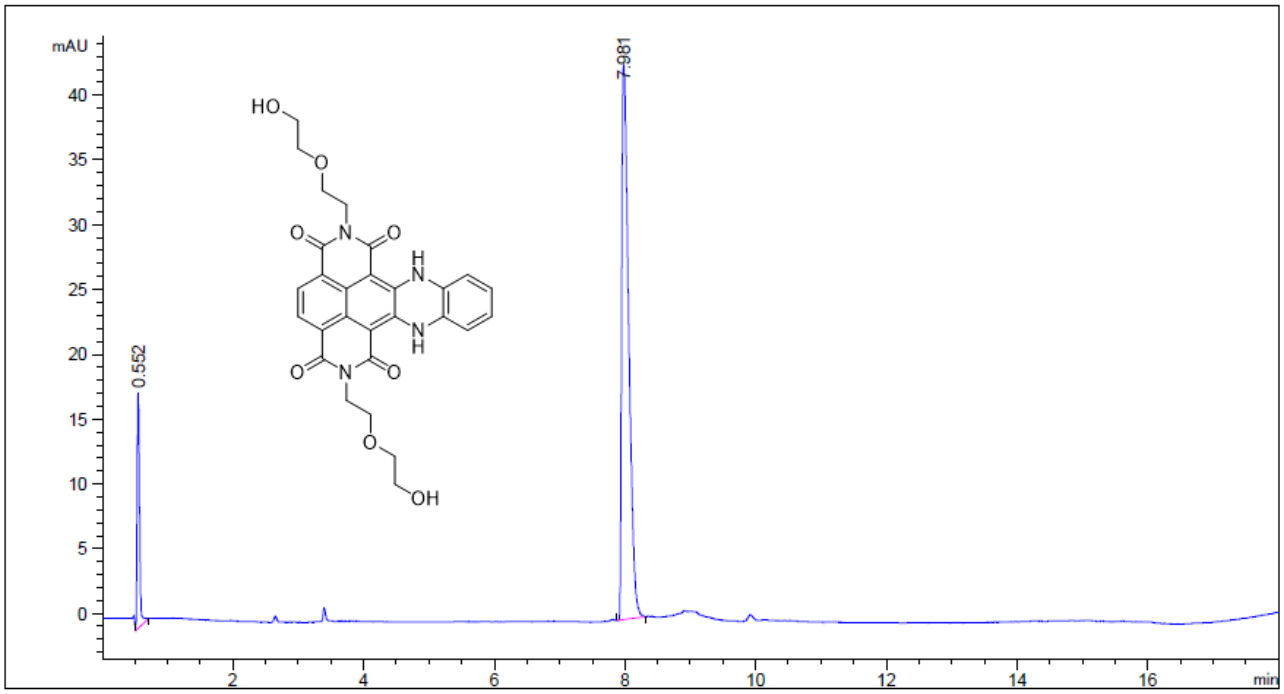

NMR characterization

Compound 2 – ^{1}H NMR

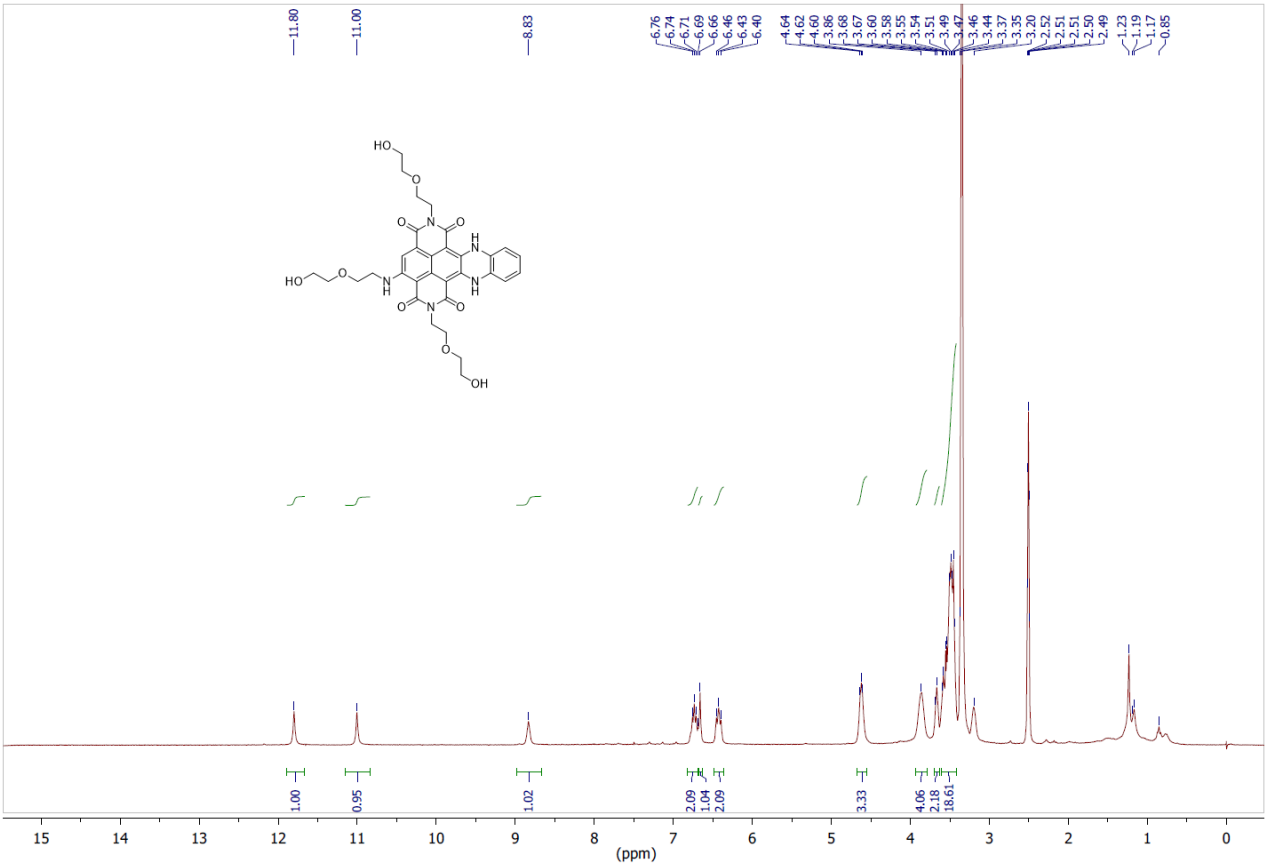

Compound 8 – ^{1}H NMR

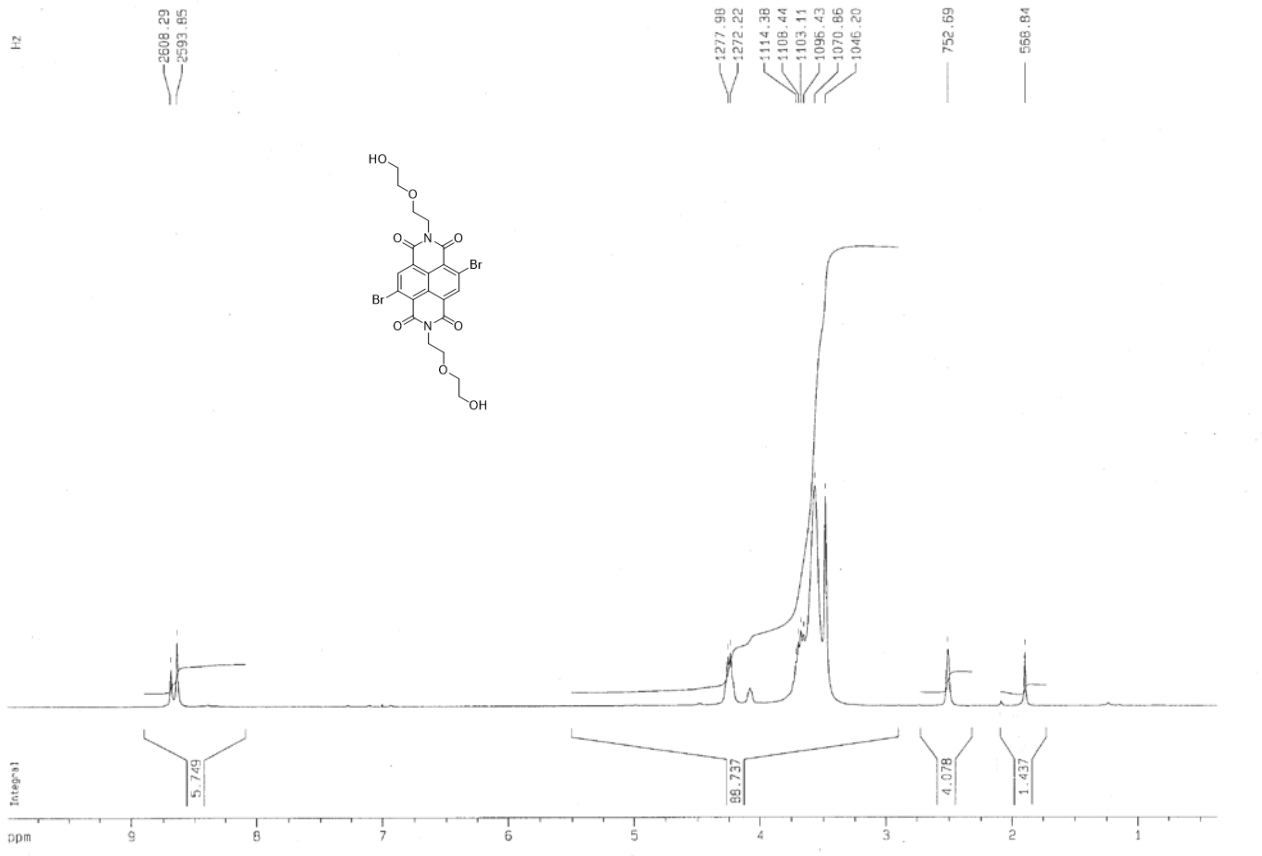

Compound 8 – ^{13}C NMR

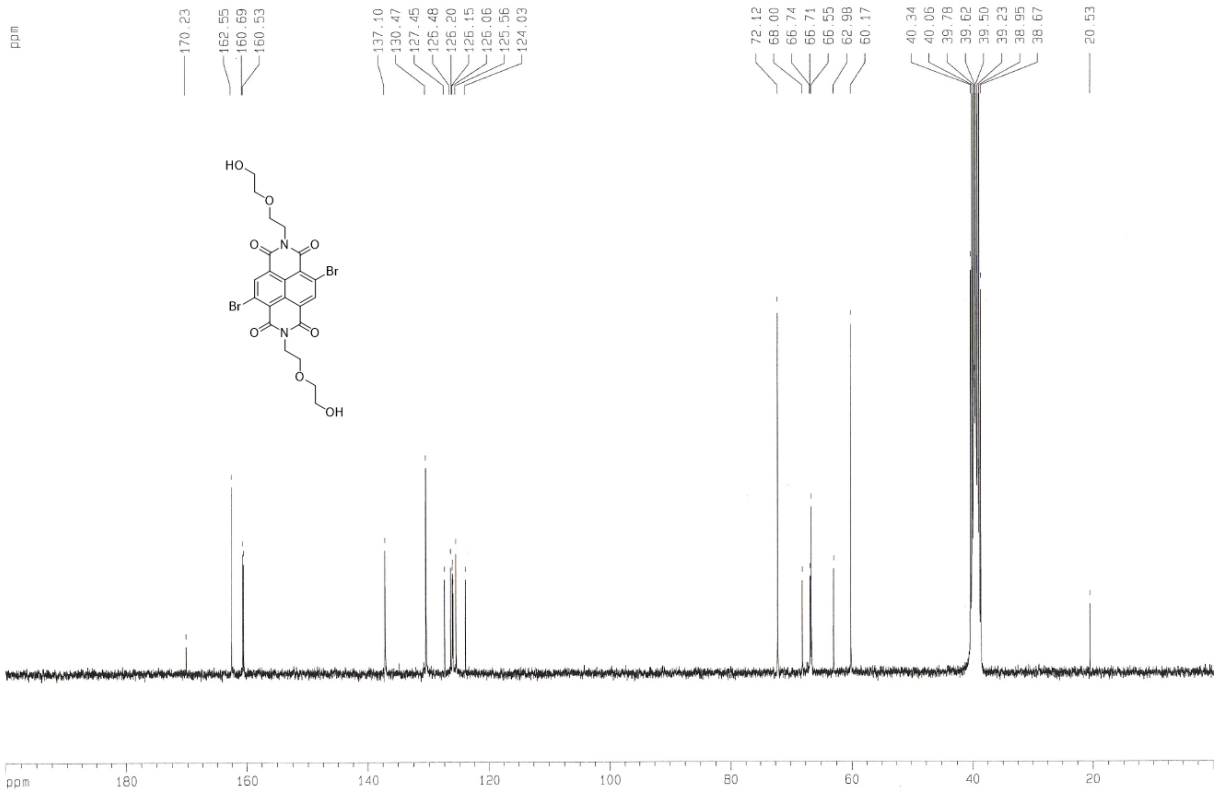

Compound 9 – ^{1}H NMR

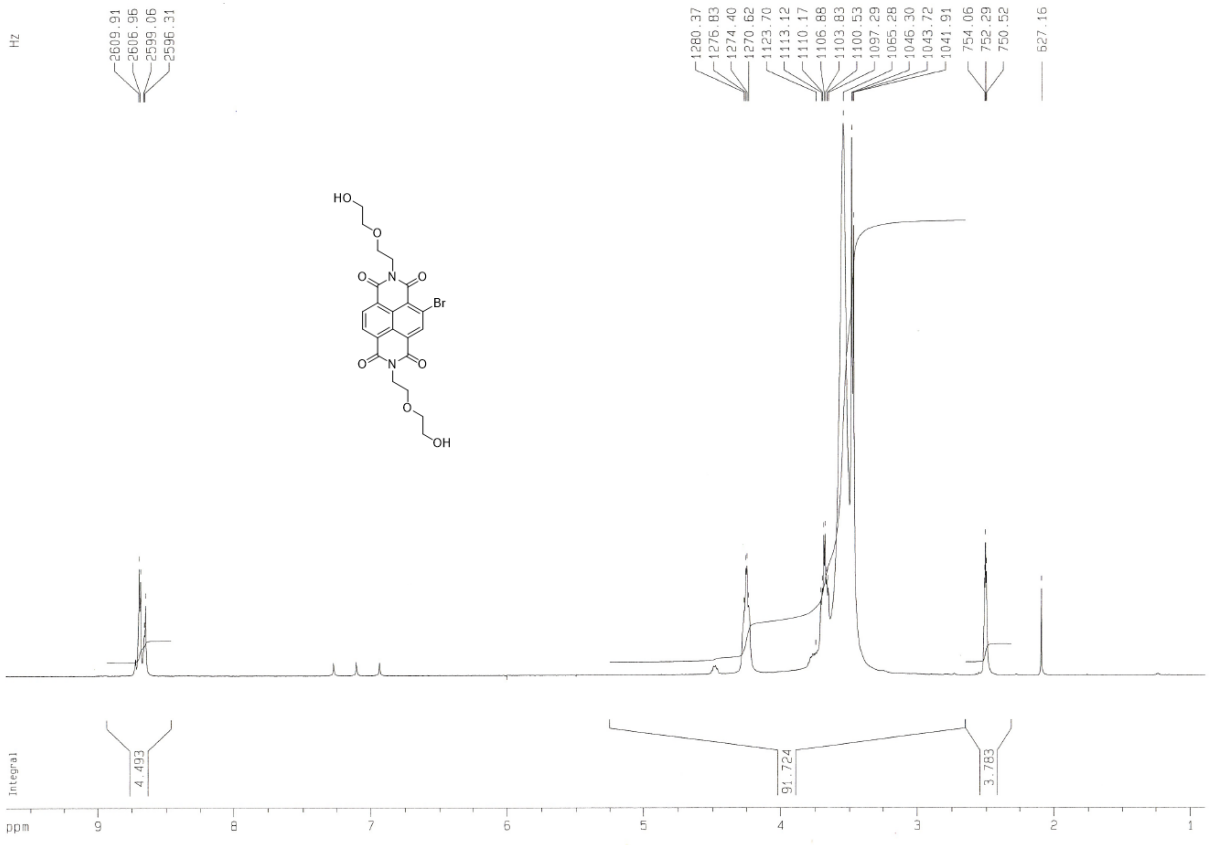

Compound 9 – ^{13}C NMR

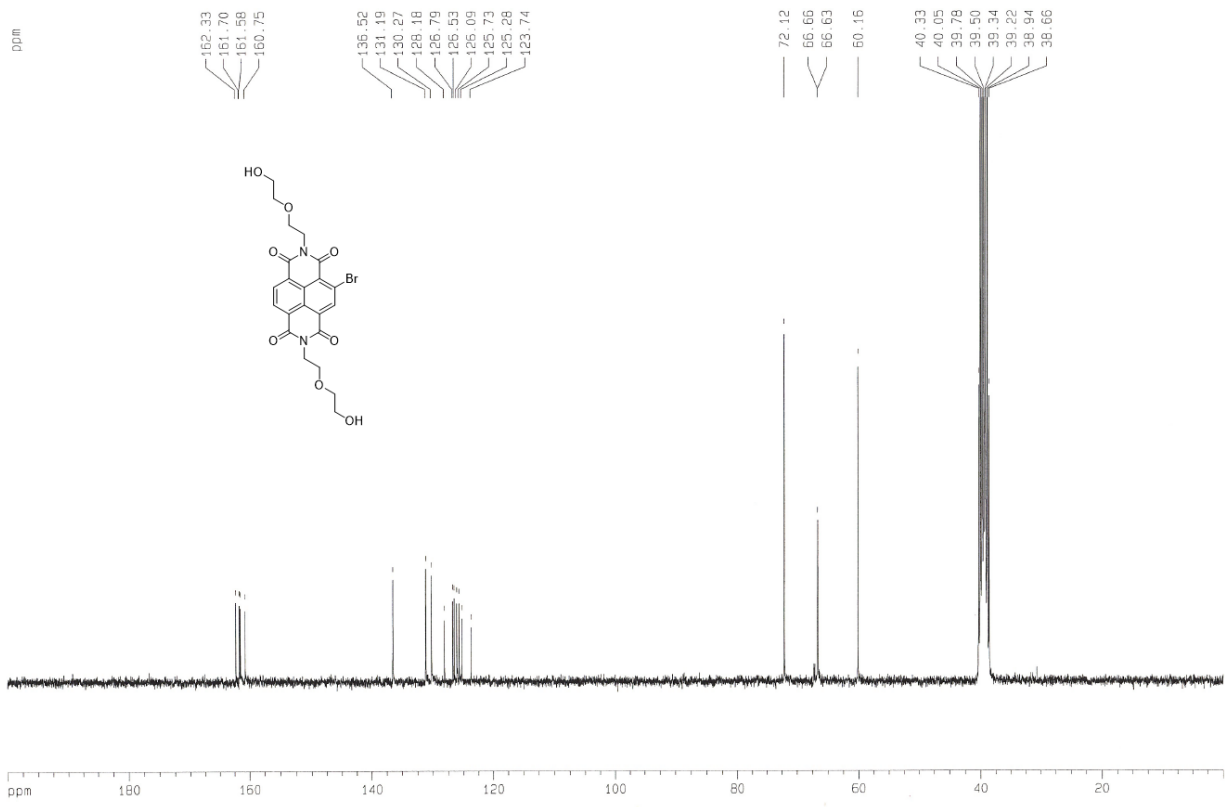

Compound 12 – ^{1}H NMR

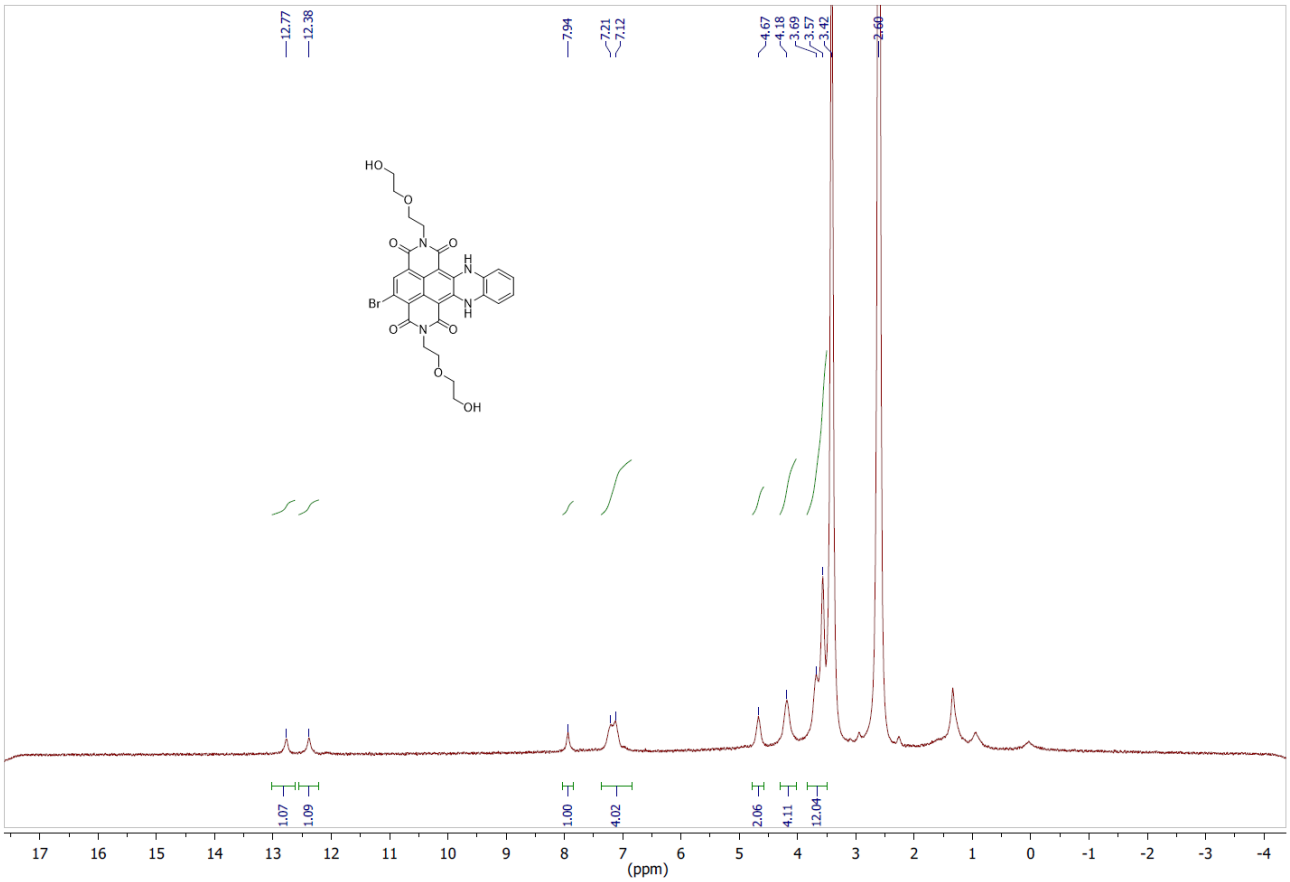

Compound 13 – ^{1}H NMR

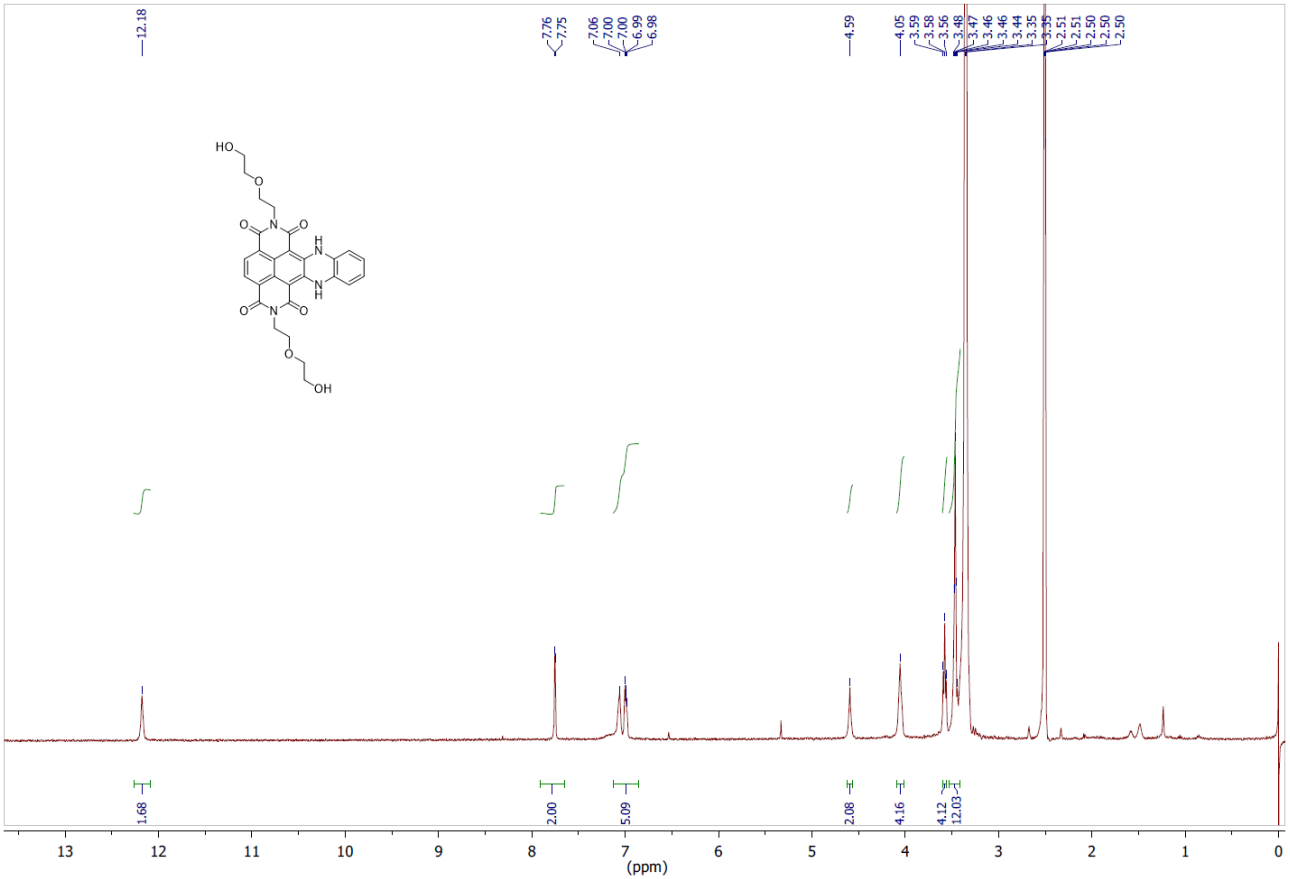

Compound 13 – ^{13}C NMR

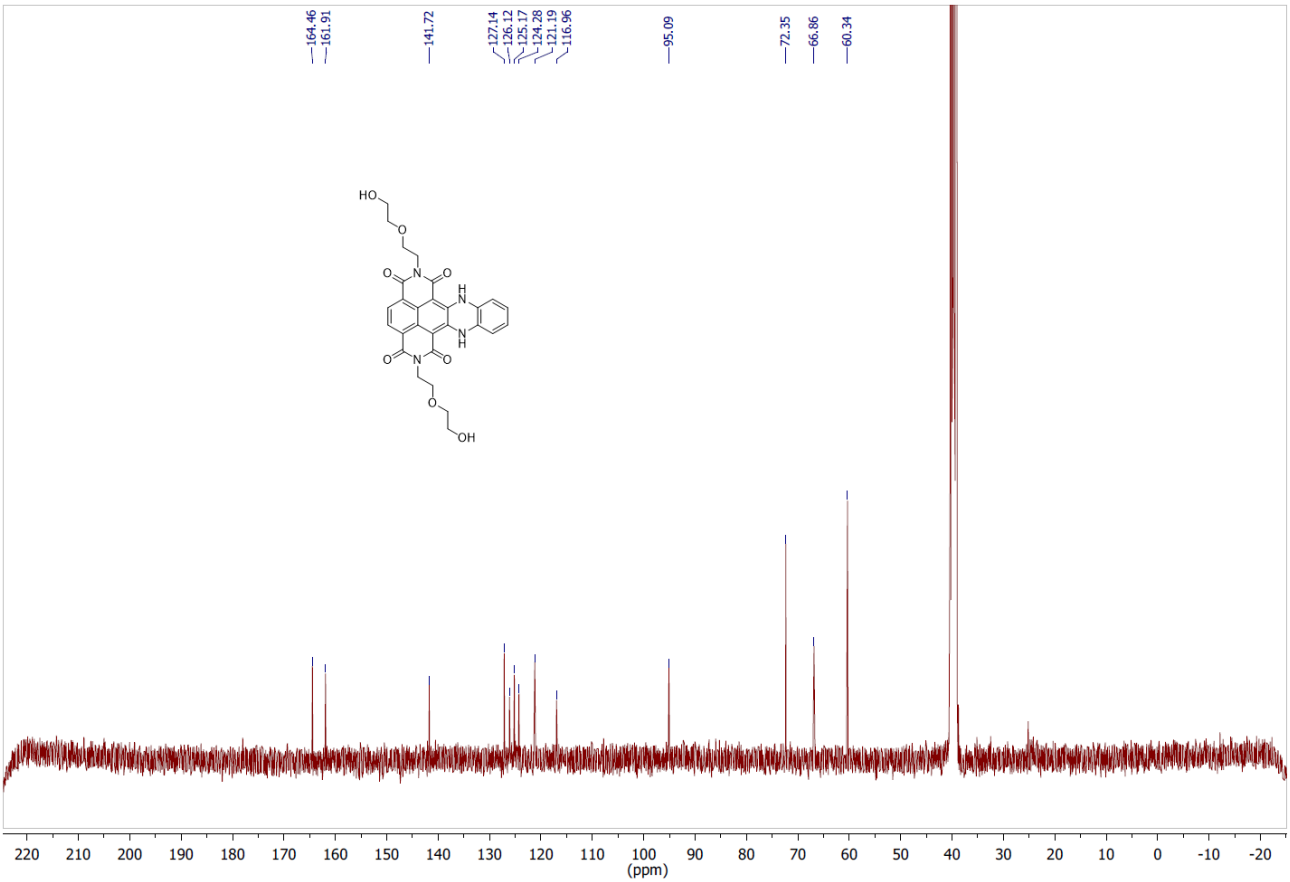

Supplementary references

1. Amrane, S., Adrian, M., Heddi, B., Serero, A., Nicolas, A., Mergny, J.-L. and Phan, A.T. (2012) Formation of Pearl-Necklace Monomorphic G-Quadruplexes in the Human CEB25 Minisatellite. *Journal of the American Chemical Society*, **134**, 5807-5816.
2. Largy, E. and Mergny, J.-L. (2014) Shape matters: size-exclusion HPLC for the study of nucleic acid structural polymorphism. *Nucleic Acids Research*, **42**, e149-e149.
3. Phan, A.T. (2010) Human telomeric G-quadruplex: structures of DNA and RNA sequences. *FEBS Journal*, **277**, 1107-1117.
4. De Rache, A. and Mergny, J.-L. (2015) Assessment of selectivity of G-quadruplex ligands via an optimised FRET melting assay. *Biochimie*, **115**, 194-202.
5. Nicoludis, J.M., Barrett, S.P., Mergny, J.-L. and Yatsunyk, L.A. (2012) Interaction of human telomeric DNA with N-methyl mesoporphyrin IX. *Nucleic Acids Research*, **40**, 5432-5447.
6. Phan, A.T., Kuryavyi, V., Gaw, H.Y. and Patel, D.J. (2005) Small-molecule interaction with a five-guanine-tract G-quadruplex structure from the human MYC promoter. *Nature chemical biology*, **1**, 167-173.
7. Kumar, N. and Maiti, S. (2008) A thermodynamic overview of naturally occurring intramolecular DNA quadruplexes. *Nucleic Acids Research*, **36**, 5610-5622.
8. Zhang, A.Y.Q., Bugaut, A. and Balasubramanian, S. (2011) A Sequence-Independent Analysis of the Loop Length Dependence of Intramolecular RNA G-Quadruplex Stability and Topology. *Biochemistry*, **50**, 7251-7258.
9. Dai, J., Carver, M., Punchihewa, C., Jones, R.A. and Yang, D. (2007) Structure of the Hybrid-2 type intramolecular human telomeric G-quadruplex in K(+) solution: insights into structure polymorphism of the human telomeric sequence. *Nucleic Acids Research*, **35**, 4927-4940.